

# Combined MEG and fMRI Model

Abbas Babajani-Feremi,<sup>1</sup>Hamid Soltanian-Zadeh,<sup>1,2</sup>

1- Image Analysis Lab., Radiology Department, Henry Ford Hospital, Detroit, MI 48202, USA

2- Control and Intelligent Processing Center of Excellence, Electrical and Computer Engineering Department, University of Tehran, Tehran 14395-515, Iran

## Abstract:

An integrated model magnetoencephalography (MEG) and functional Magnetic Resonance Imaging (fMRI) is proposed. In the proposed model, MEG and fMRI outputs are related to the corresponding aspects of neural activities in a voxel. Post synaptic potentials (PSPs) and action potentials (APs) are two main signals generated by neural activities. In the model, both of MEG and fMRI are related to the PSPs without any correlation to the APs. Each PSP is modeled by the direction and strength of its current flow, which are treated as random variables. The overall neural activity in each voxel is used for equivalent current dipole in MEG and as input of the extended Balloon model for producing Blood Oxygen Level Dependent (BOLD) signal in fMRI. The proposed model shows possibility of detecting activation by fMRI in a voxel while the voxel is silent for MEG and vice versa. This is according to the fact that fMRI signal reflects the sum of PSPs' strengths (independent of their directions) but MEG signal reflects the vector sum of the PSPs (which depends on their directions). The model also shows that the crosstalk from neural activities of adjacent voxels in fMRI and properties of the inverse problem in MEG generate different spatial responses in the two modalities.

We use real auditory MEG and Fmri datasets from 2 normal subjects to estimate the parameters of the model. Goodness of the real data our model shows the possibility of using the proposed model to simulate realistic datasets.

**Keywords:** Blood Oxygen Level Dependent (BOLD); Equivalent Current Dipole (ECD); Post Synaptic Potential (PSP); Action Potential (AP); extended Balloon model.

## 1- Introduction

In another work, David *et al.* in [10] propose an extended neural mass model based on the

In recent years, numerous efforts have been directed at multimodal data fusion. Electroencephalography (EEG), magnetoencephalography (MEG), and functional Magnetic Resonance Imaging (fMRI) are innovative functional brain imaging techniques. The spatiotemporal resolution of these techniques is different. EEG and MEG have good temporal resolutions in the order of millisecond, but their spatial resolutions are poor due to ill-posedness of the inverse solution. On the other hand, fMRI has good spatial resolution in the order of millimeter but poor temporal resolution due to the limited rates of the image acquisition methods and change in the hemodynamic response. Since M/EEG and fMRI are different views of a common source (neural activity), their integrated analysis should improve the overall spatiotemporal resolution. Several sophisticated methods have been introduced for M/EEG and fMRI combined analysis [9,1,25,30] in order to extract as much information as possible using a data-driven strategy (the authors refer to them as top-down methods).

Although integrated M/EEG and fMRI model (bottom-up modeling) is an active area of research, there is limited work about it in the literature [5,37,38,40]. We introduce an integrated model [5] based on the physiological principles of the cortical minicolumns and their connections. In the integrated model, we use our proposed extended neural mass (ENM) model to generate MEG/fMRI signals. In this model, MEG signals are generated by synaptic activations of the pyramidal cells and sub-sequential currents in minicolumns that have been collectively modeled as an equivalent current dipole (ECD). We extract the fMRI signal from the proposed extended neural mass model by introducing a relationship between the stimulus and the overall neural activity and using it as the input of the EBM. By comparing the simulation results with the experimental results, we validate the proposed model.

Janssens model [21] to generate EEG/MEG data. They consider multiple cortical areas with Bottom-up, Top-down and Lateral connections between

them. Then, they estimate parameters of their model using real auditory and visual data [11]. It is noticeable that although the model proposed in [10] is based on neural mass, but their model is not an integrated EEG/MEG and fMRI model. Sotero and Trujillo-Barreto propose an integrated EEG/fMRI model based on neural mass [40]. They use Jansen's model as the base of their neural mass model and derive the relationship between inhibitory and excitatory activities with the resultant BOLD and EEG signals. The effects of the inhibitory and excitatory activities on the resultant BOLD signal are different in their model. They consider the neural mass model in each voxel which describes the neuronal dynamics within the voxel. By defining short-range interactions (connection within an area) and long-range interactions (inter area connection), they generate EEG and fMRI signals of the whole brain.

In the integrated model proposed by Riera, *et al.* [36,38], a two-dimensional autoregressive model with exogenous variables (ARx) is proposed to describe the relationships between synaptic activity and hemodynamics. They use a static nonlinear function to describe the electro-vascular coupling through a flow-inducing signal. In this work, a linear relationship between cerebral blood flow (CBF) and Blood Oxygen Level Dependent (BOLD) is assumed which is not generally valid [7].

In this paper, we propose an integrated model totally different from the integrated model in [38] and does not have its limitation. As mentioned in the previous paragraph, the main limitation of the Riera's model is related to this fact that considering linear relationship between CBF and the BOLD signal does not generally correct. The nonlinear relationships among CBF, cerebral blood volume (CBV), and the resultant BOLD signal are formulated in Balloon model in [7]. Friston and his colleagues proposed the extended Balloon model [13] and added a model of CBF changes to the Balloon model, based on synaptic activation and CBF autoregulation. We use the extended Balloon model in our proposed model to remove the limitation of the Riera's model.

The proposed model is consistent with the fact that fMRI signal reflects the sum of PSPs' strengths (independent of their directions) but MEG signal reflects the vector sum of the PSPs (which depends on their directions). The model also shows that the crosstalk from neural activities of adjacent voxels in fMRI and properties of the inverse problem in MEG generate different spatial responses in the two modalities. These are illustrated by the simulation studies in this paper. For validation of the proposed model in real conditions, we use real auditory MEG and fMRI datasets from 2 normal subjects to estimate the parameters of the model. Goodness of fit of the real data with our model suggests that the proposed model can be used in real conditions.

It should be noted that whenever we refer to the direction of the PSP, it is scientifically better to use PSC (postsynaptic current) instead of PSP (postsynaptic potential). However, since many of the MEG literature use PSP instead of PSC and also the direction of PSC is

not important for fMRI, we use PSP throughout this paper. The organization of the rest of the paper is as follows. The background material and details of the proposed model are described in Section II. Analysis of proposed model is presented and discussed in Section III. Estimation of the parameters of the model using real auditory datasets is presented in Section IV. Conclusions are given in Section V.

## 2. Proposed Combined MEG/fMRI Model

Neuron is the principal building block of the brain. The overall activities of adjacent neurons in a region can be detected by MEG or fMRI. In the proposed model, the activities of neurons in a voxel are used for constructing MEG and fMRI signals. A voxel in the order of  $1 \text{ mm}^3$  contains approximately  $10^5$  pyramidal cells and thousands of synapses per neuron [15]. Activity of each neuron starts with activities of its synapses that produce PSPs. The overall activities of synapses may produce action potentials (APs). PSPs and APs are two main indices for showing neural activities. MEG and fMRI are related to neural activities and thus to the PSPs and/or the APs.

The proposed integrated model is constructed based on the principle that PSPs are the main link between the two techniques. We construct a stochastic model for PSPs so that each parameter (like direction and strength of PSPs) has a probability density function (pdf). The input of the model is the waveform of the external stimulation (Fig. 1). The number of PSPs at each time is constructed with a stochastic model according to the waveform of the input stimulus. The MEG signal is produced according to the pdfs of the direction and strength of the PSPs. The BOLD signal only depends on the overall strengths of PSPs, which is the input of the extended Balloon model for producing the BOLD signal. The overview of the relevant previous work and physiological principles underlying the proposed integrated model is presented in the following subsection before introducing the model.

### 2.1. Physiological Bases of MEG and fMRI

Compartments of a neuron are the soma, the dendrites, and the axon. The soma (the cell body) contains the nucleus and much of metabolic machinery. The stimuli from other cells are received by synapses on the dendrites. The axon is a single long fiber that carries the nerve impulse away from the soma to other cells (see Fig. 2). There are typically thousands of synapses (connections) from other neurons in the dendrites and soma. The intracellular potential increases by input through the excitatory synapses called excitatory post synaptic potential (EPSP), but decreases by inhibitory input called inhibitory post synaptic potential (IPSP). When the potential at the axon hillock reaches a certain threshold level, the neuron fires an action potential (AP).

The peak value of each PSP is in the order of 10 mV and has a duration of approximately 2-10 ms. For the AP, the peak value is in the order of 100 mV and its duration is approximately 1 ms [15].

The relationship between PSPs and APs with MEG and BOLD signals is inferred in this section. First, we deal with the MEG signal. Both action and synaptic currents generate magnetic fields. Approximately, the action potential can be considered as two opposite oriented current dipoles, which form a current quadrupole. The magnetic field produced by a quadrupole of AP decreases as  $1/r^3$  where  $r$  is the distance between dipole and detection sensor. However, the magnetic field produced by a PSP is dipolar and decreases as  $1/r^2$ . Moreover, longer duration of a PSP (tens of ms) allows more effective temporal summation of neighboring currents than with the 1 ms lasting APs. Thus, the MEG signals are likely produced by the synaptic current flow [15]. It is also reported in other papers [4,35] that PSP is the main source of the MEG signal. Thus, we only consider the effect of PSP on the MEG signal and ignore the effect of AP.

Now, the relationship between the BOLD signal and the neural activities (PSPs and/or APs) is discussed. This relationship has been addressed experimentally in a number of studies [16,27,28,29,36,41]. Logothetis and colleagues have done many experimental studies for illustrating the relationship between BOLD signal and PSPs (synaptic activities) or APs (spike activities) [27,28,29]. They use especial instruments for high spatiotemporal resolution fMRI. They achieve the resolution of  $75 \times 150 \times 300 \mu\text{m}^3$  which reflects the activity of as few as 600-1200 cortical neurons. They simultaneously gather BOLD signal and neural electrical activities with microelectrode and then separate two types of neural signals (MUA and LFP) based on their different frequency characteristics. The Multiple Unit spiking Activities (MUAs) are a weighted sum of the extracellular APs and the Local Field Potentials (LFPs) are the weighted average of synchronized dendro-somatic components of the synaptic signals. Thus, MUAs and LFPs are similar to the APs and PSPs, respectively. In an experimental study, Logothetis and colleagues did the experiment on 10 monkeys with elicited visual cortical responses to a checkerboard pattern using a block design [29]. They saw that although MUA rises after activation, but it returns to baseline after 2-4 sec. Conversely, LFP was always elevated for the duration of the stimulus, similar to the BOLD signal. Both BOLD and LFP increased when the contrast of checkerboard stimuli increased, but the relation between BOLD and LFP remained nonlinear. They concluded that the LFPs were the only neural signals associated with the BOLD response.

Lauritzen and Gold have summarized results from several experimental studies [24]. They used the rat cerebellar cortex for detailed studies of the relationship among AP, synaptic activity, and changes in CBF. Their final result implies that it is impossible to conclude whether the spike

activity (or AP) in a given brain region is increased or decreased on the basis of increases in CBF (and consequently the BOLD signal). They report that the CBF or BOLD increases when the LFP is increased and the relation between LFP and CBF is an increasing function that may be nonlinear. This also indicates that PSPs affect the BOLD signal.

In addition to the above, we can verify the relation between the BOLD and the AP or the PSP with a structural neurovascular coupling view. The average activity in a given region largely correlates with the density of the vascular network in the region. Most investigators report high spatial correlations between vascular density and the number of synapses rather than the number of neurons [28]. The human cortical vascular network can be subdivided into four layers parallel to the surface. The vascularization of Lamina IVc (layer 4, part c) is the highest and that of Lamina I (layer 1) is the lowest. The average IVc/I ratio across animals is approximately 3. On the other hand, in the striate cortex of macaque the IVc/I ratio of synaptic and neurons densities are 2.43 and 78.8, respectively [28]. This implies that the vascular density is correlated with the density of perisynaptic elements (sources of PSPs) rather than that of neuronal somata (sources of APs).

Relation between BOLD and PSP can be verified from brain energy metabolism. Attwell and Iadecola [3] reported the allotment of energy consumption in primate for post synaptic potential, pre synaptic terminals, action potential, glia and resting potential as 75%, 7%, 10%, 6% and 2%, respectively. Thus, the main part of energy is consumed by PSP. Since the blood flow increases in proportion to the energy consumption [17], PSP has the highest correlation with BOLD signal compared to the others.

EPSP and IPSP have different polarizations and therefore canceling effects for MEG. Do they have same effect on the BOLD signal in fMRI? Experimental study of Caesar and colleagues is one of the newest studies that answer this question [8]. They performed experiments in 10 male Wistar rats and recorded the single-unit spiking activities (APs) and local extracellular synaptic field potentials (LFPs) of Purkinje cells in the cerebellar cortex with a single electrode at a depth of 300-600  $\mu\text{m}$  of vermis segments 5 and 6. They stimulated the cerebellar climbing fibers (CF; excitatory) and parallel fibers (PF; inhibitory) alone and in combination and simultaneously recorded the rCBF in the Purkinje cells. They reported that stimulation of the excitatory climbing fiber (EPSP) or inhibitory parallel fibers (IPSP) increases the CBF amplitude and there is no any difference between EPSP and IPSP in this regard. Thus, they concluded that the EPSP and IPSP have similar effects on the BOLD signal. In summary, considering the above facts and experimental studies, we conclude that both of equivalent current dipole (ECD) in MEG and BOLD signal in fMRI are mainly correlated to the PSPs and it is reasonable to ignore the effect of APs. The BOLD is an increasing but nonlinear function of PSPs. Although EPSP and IPSP

have opposite effects in MEG, both of them have the same increasing effect on BOLD signal. We have used these facts for constructing the proposed model (see below).

## 2.2. Details of Proposed Model

The proposed model relates the MEG and fMRI signals in an active voxel of the brain. There are a huge number of neurons and synapses in a voxel. If during external stimulation a voxel belongs to the active region of the brain, there are many PSPs and APs in this voxel whose numbers and strengths show the rate of neural activities. According to our discussion in the previous section, we consider the PSPs as the single link between MEG and fMRI in the proposed model and ignore the effects of APs. The number and strengths of PSPs show the overall neural activities that produce MEG signal and change the blood flow for producing BOLD signal as shown in Fig. 1. The proposed model contains multiple blocks, which we will discuss in the following subsections.

## 2.3. PSP Production Mechanism

In each voxel, there is a network of neurons that have many interconnections (by synapses) and may have inputs from peripheral nerves or neurons in the neighboring voxels. After external stimulation, the activation in a voxel will start from activation of neurons that have peripheral nerve inputs or input connections with active neurons of another voxel. Gradually the number of active PSPs (also active neurons) in a voxel increases to its maximum number when most of the interconnection synapses are activated. After this time, it is logical to say that the number of active PSPs does not almost change during the stimulation and this maximum number depends on the strength of the external stimulation.

Block 1 of Fig. 1 implements the relationship between the external stimulus and the number of active PSPs. The number of active PSPs at each time point is assumed as the output of a linear system whose input is the external stimulus, similar to the linear model relating the external stimulus to the evoked transient in [37].

$$\sum_{k=0}^r \alpha_k \frac{d^k N(t)}{dt^k} = N_{ss} Stm(t - t_{af}) \quad (1)$$

where  $t_{af}$  is the delay due to different relay processes in the long afferent pathways. The first order linear model with  $\alpha_0 = 1$  and  $\alpha_1 = 50$  ms is used as the simplest linear model. For block design,  $Stm(.)$  is the unit function and  $N_{ss}$  is the steady state value of the  $N(t)$ . For event related design,  $Stm(.)$  is the Dirac delta function and  $N_{ss} / \alpha_1$  is the peak value of  $N(t)$ . Physiological noise is modeled by  $\varepsilon(t)$  in Fig. 1 and represents the number of active PSPs, which is not related to the external stimulus and is related to the spontaneous activity. It can be modeled as a

Poisson process.

## 2.4. Extracting Relationship Between fMRI and PSPs

The second block of the model (Fig. 1) shows the relationship between different aspects of PSPs and MEG or fMRI. Each PSP is like a small current dipole, a vector with direction and magnitude. Both direction and magnitude of this vector are important for MEG, but only magnitude is important for fMRI. The magnitude or strength of each PSP depends on the kind of neuron, synapse, and dendrite parameters. In addition, direction of the current dipole for each PSP depends on the shape and structure of dendrite trees. Since there are no deterministic models for these parameters, we consider them as random variables in the proposed model.

The kind of PSP (IPSP or EPSP) is important for MEG because of their opposite polarities, but is not important for fMRI according to our previous discussions. The total number and ratio of excitatory and inhibitory synapses are different in different regions of the brain, but the number of excitatory synapses generally is more than inhibitory synapses [14]. The single pyramidal cell has about 12 mm dendrites and receives around 30,000 excitatory and 1,700 inhibitory inputs in rat hippocampal CA1 area [32]. We consider the ratio of IPSP number to all PSP as a parameter in our model and change it for verifying its effect on MEG.

The relationships between produced PSPs and MEG or fMRI signals are illustrated in block 3 of Fig. 1. We start discussing the fMRI part of the model followed by the MEG part. The first block in the fMRI part of the model is "Crosstalk from Neural Activities of Adjacent Voxels." Neural activities in a voxel change the blood flow of this voxel and also can affect the blood flow of the adjacent voxels. In an experimental study on rats, it is reported that the diameter of local arterioles (at the stimulation site) increases 26% and local blood flow increases 55% while in an up stream region with a distance of about 2 mm from the stimulation site, the diameter of arterioles increases 8.7% and blood flow increases 15% [20]. In another experimental study on rats with electrical stimulation of the cerebellar parallel fiber, the local CBF at the stimulation site changes 55% while at sites with 4.5 mm horizontal and 1 mm vertical distance from the stimulation site, CBF changes 13% and 11%, respectively [19]. Thus, the synaptic activities in a voxel can affect the CBF and resultant BOLD signal in adjacent voxels.

The Gaussian spatial smoothing function is used for modeling the spatial crosstalk of BOLD signal in our proposed model. We consider the effective synaptic activities as below:

$$\begin{cases} u_e(r; t) = G(r) * u(r; t); & r = (x, y, z) \\ G(r) = \frac{1}{\sigma_x \sigma_y \sigma_z (2\pi)^{3/2}} \exp\left(-\frac{x^2}{2\sigma_x^2} - \frac{y^2}{2\sigma_y^2} - \frac{z^2}{2\sigma_z^2}\right) \end{cases} \quad (2)$$

where  $u(r; t)$  is synaptic activities in the voxel located at

$r(x,y,z)$ ,  $G(r)$  is a 3D Gaussian kern and “\*” shows 3D convolution.  $\sigma$  in (2) is the only fMRI parameter in the model that can show the difference between fMRI and MEG spatial responses as discussed in the next section. We use the reported data from [19,20] and estimate  $\sigma$  with curve fitting of the reported data into a 3D Gaussian function. The estimated  $\sigma$  is 2.6 mm in the horizontal direction (axial slice) and 0.7 mm in the vertical direction (normal to axial slice) of the brain.

The “extended Balloon model” is used as the main mechanism for relating PSPs as the neural activity input and BOLD signal as the output. The Balloon model was originally proposed by Buxton and colleagues [Buxton et al., 1998]. In this model, a model of oxygen exchange is linked to the venous dilation processes due to CBF variations, and the BOLD signal is derived from the total deoxyhemoglobin content within a voxel. Friston and colleagues [13] added a model of CBF changes to this Balloon model, based on synaptic activation and CBF autoregulation. We use this extended Balloon model in our proposed model.

In the extended Balloon model, the neural activity  $u(t)$  is related to the BOLD signal  $y(t)$  by the following equations:

$$\begin{cases} \dot{s} = \varepsilon u(t) - s / \tau_s - (f_{in} - 1) / \tau_f \\ \dot{f}_{in} = s \end{cases} \quad (3)$$

$$\begin{cases} E(f_{in}, E_0) = 1 - (1 - E_0)^{1/f_{in}} \\ \tau_0 \dot{v} = f_{in} - f_{out}(v) \quad , \quad f_{out} = v^{1/\alpha} \\ \tau_0 \dot{q} = f_{in} \frac{E(f_{in}, E_0)}{E_0} - f_{out}(v)q/v \end{cases} \quad (4)$$

$$y(t) = V_0 \left\{ \frac{7E_0(1-q) + 2(1-q/v) + }{(2E_0 - 0.2)(1-v)} \right\} \quad (5)$$

where  $V_0$  is resting blood volume fraction,  $E_0$  is resting net oxygen extraction fraction by the capillary bed,  $v$  is normalized venous volume,  $q$  is normalized total deoxyhemoglobin voxel content,  $f_{in}$  and  $f_{out}$  are inflow and outflow from the venous compartment,  $s$  is some flow inducing signal, and there are four fixed parameters that must be estimated. The mean values of these parameters are  $\varepsilon = 0.5$ ,  $\tau_s = 0.8$ ,  $\tau_f = 0.4$ ,  $\tau_0 = 1$ ,  $\alpha = 0.2$ . We consider  $V_0 = 0.02$  and  $E_0 = 0.8$  in our simulations according to [13].

Input of the extended Balloon model is the overall synaptic activities which are linearly related to the regional cerebral blood flow. To find a relationship between synaptic activity and PSPs, we note the following. Each PSP consumes a little energy and causes a small change in the blood flow. Thus, it is logical to consider synaptic activity (as input of the extended Balloon model) proportional to the total consumed energy by the PSPs. We need to solve the Hodgkin-Huxley (H-

H) equation for computing the voltage, current and energy of PSP. The PSP’s voltage is modeled by multiplying a constant peak value  $\Delta V$  and a normalized waveform  $\varphi(t)$  [Almeida and Stetter, 2002; Larkum et al., 1998]:

$$\varphi(t) = \frac{t e^{-\frac{(t-\tau_{PSP})}{\tau_{PSP}}}}{\tau_{PSP}} \quad (6)$$

$$V(t) = \Delta V \varphi(t) \quad (7)$$

where  $\tau_{PSP}$  is time constant of  $\varphi(t)$  and is considered as a random variable with truncated Gaussian distribution  $\tau_{PSP} \sim TN(2,1; 0, \infty)$  ms according to the data reported in [12]. The truncated Gaussian variable denoted by  $x \sim TN(\mu, \sigma; a, b)$  is a variable whose probability for  $x < a$  or  $x > b$  is zero and its pdf is like the Gaussian distribution (except for a scalar normalization) in the interval  $x \in [a, b]$  with mean  $\mu$  and standard deviation  $\sigma$ .

The consumed energy by PSP is found by:

$$E = \int_0^{\infty} V(t).I(t)dt \quad (8)$$

where  $I(t)$  is postsynaptic current. For simplicity,

we use a constant value for  $I(t)$  and according to (6)-

(8) get:

$$E = I \tau_{PSP} \Delta V \quad (9)$$

If  $N(t)$  PSPs fire at time  $t$ , the consumed energy for each of them is represented by (9). The neural activity should be proportional to the sum of the consumed energies. Therefore, the following equation relates the synaptic activity (or neural activity)  $u(t)$  to the parameters of the PSPs:

$$\begin{cases} E = \sum_{k=1}^{N(t)} E_k = \sum_{k=1}^{N(t)} I \tau_{PSP}^k \Delta V_k \propto \sum_{k=1}^{N(t)} \tau_{PSP}^k \Delta V_k \\ u(t) \propto \sum_{k=1}^{N(t)} \tau_{PSP}^k \Delta V_k \end{cases} \quad (10)$$

The temporal resolution of MEG is in the order of ms and so we choose the sampling time of 1 ms for synaptic activities in our model. Thus, the sampling time of BOLD output in the Balloon model is 1 ms. With conventional imaging systems, the temporal resolution of the BOLD signal is in the order of seconds. The output of the Balloon model is down sampled and shown by “Down Sampling” box in Fig. 1. We choose the rate of 1 ms/2 s down sampling in the simulations.



## 2.5. Extracting Relationship between MEG and PSPs

From a distance, the PSP looks like a current dipole oriented along the dendrite. Approximately, the current dipole according to PSP is [15]:

$$\vec{q} = \frac{\pi}{4} d^2 \sigma_{in} \Delta V \cdot \vec{n} \quad (11)$$

$$\vec{q} = \beta \Delta V \cdot \vec{n} \quad , \quad \beta = \frac{\pi}{4} d^2 \sigma_{in} \quad (12)$$

where  $d$  is the diameter of the dendrite,  $\sigma_{in}$  is the intracellular conductivity,  $\Delta V$  is change of voltage during PSP and  $\vec{n}$  is the unit vector showing current dipole orientation along the dendrite. Using the typical values  $d = 1 \mu\text{m}$ ,  $\sigma_{in} = 1 \Omega^{-1} \text{m}^{-1}$  and  $\Delta V = 25 \text{mV}$  from [Hämäläinen et al., 1993], we calculate  $q \approx 20 \text{fAm}$  for a single PSP.

There are many types of neurons with different shapes and sizes of dendritic tree (Fig. 3). The pyramidal cells (Figs. 1 and 3-d) are relatively large. Their apical dendrites are parallel to each other and tend to be perpendicular to the cortical surface [15]. Since the apical dendrites of pyramidal cells are parallel, their current dipoles of PSPs can be summed effectively. The dendrites of Purkinje cells (Fig. 3-e) are not unidirectional and so the current dipoles at different branches of their dendrites may cancel each other. We consider a random variable for the direction of current dipoles (of PSP) for modeling different kinds of neurons and dendrite tree structures.

We define "reference vector" as a vector that is perpendicular to the cortical surface in each voxel. The angle between the reference vector and each current dipole ( $\theta$ ) is considered as a truncated Gaussian random variable with the following pdf:

$$f_{\theta}(\theta) = \frac{e^{-\frac{\theta^2}{2\sigma^2}}}{\sigma \sqrt{2\pi}} \quad ; \quad k = \sqrt{2\pi} \quad (13)$$

where  $erf(\cdot)$  is the error function. The pdf of  $\theta$  is shown in Fig. 4 for some values of  $\sigma$ . The current dipole  $q$  in (12) is projected onto two vectors, first vector ( $q_p$ ) is parallel to the reference vector with the value of  $q \cos(\theta)$  and the second vector ( $q_n$ ) is orthogonal to the reference vector with the value of  $q \sin(\theta)$ . The  $E[q_n]$  is zero (due to odd property of  $\sin(\cdot)$  and even property of  $f_{\theta}(\theta)$  in (13)), thus,  $q_n$  acts as a noise for MEG sensors having no correlation with the stimulation. On the other hand, the  $E[q_p]$  is nonzero and can be sensed by the MEG sensors

as a signal. When  $\sigma \rightarrow \infty$  in (13), distribution of  $\theta$  tends to uniform distribution and then  $E[q_p] \rightarrow 0$ . This condition models neurons like Purkinje cells with random direction of its dendrites. If  $\sigma \rightarrow 0$ ,  $\theta$  has a distribution concentrated around the reference vector. The pyramidal cells can be modeled with this condition where  $E[q_p]$  generates a strong signal highly correlated with the stimulation and detectable by the MEG sensors.

If  $N$  PSPs of the pyramidal cells fire at time  $t$ , then the ECD from the sum of their activities according to (12) is:

$$\vec{q}(t) = \sum_{k=1}^N w_k \beta_k \Delta V_k \varphi_k(t) \cdot \vec{n}_k \quad (14)$$

where  $w_k$  is +1 for EPSP and -1 for IPSP,  $\Delta V_k$  shows the peak value of PSP,  $\beta_k$  is a coefficient according to (12) that models parameters of the  $k$ th synapse and its neighboring dendrite and  $\varphi_k(t)$  is unitary peak waveform for the  $k$ th PSP at time  $t$  according to (6). For modeling different kinds of synapses, we consider  $\beta_k$  and  $\Delta V_k$  as random variables using truncated Gaussian and uniform distributions. The pdf of the uniformly distributed random variable denoted by  $x \sim \text{uniform}(a,b)$  is constant in the interval of  $[a,b]$  and zero elsewhere. We assume  $\Delta V_k$  as a truncated Gaussian distribution ( $\Delta V_k \sim TN(10,5; 0, \infty) \text{mV}$ ) [12] and  $\beta_k$  according to (12) as a function of two random variables ( $d \sim \text{uniform}(0.1,2) \mu\text{m}$  and  $\sigma_{in} \sim \text{uniform}(0.1,2) \Omega^{-1} \text{m}^{-1}$ ), based on the typical values of  $d = 1 \mu\text{m}$  and  $\sigma_{in} = 1 \Omega^{-1} \text{m}^{-1}$  [15].

The number of pyramidal PSPs in a voxel that start to fire at time  $t$  is considered as  $N(t)$ . We sample  $N(t)$  every millisecond in the simulations. The ECD in this voxel is derived from (14):

$$\vec{Q}(t) = \sum_{d=0}^D \sum_{k=1}^{N(t-d)} w_k \beta_k \Delta V_k \varphi_k(t+d) \cdot \vec{n}_k \quad (15)$$

where  $\varphi_k(t+d)$  is the waveform of the  $k$ th PSP whose activation started at the previous  $d$  sample time and  $D$  is the maximum duration of PSP which we set at  $D = 30 \text{ms}$  according to the maximum value of  $\tau_{PSP}$  in (6). The projections of  $\vec{Q}(t)$  onto two normal vectors can be found as:

$$\begin{cases} \vec{Q}(t) = [ \sum_{d=0}^D \sum_{k=1}^{N(t-d)} w_k \beta_k \Delta V_k \varphi_k(t+d) \cos(\theta_k) ] \cdot \vec{n}_p \\ + [ \sum_{d=0}^D \sum_{k=1}^{N(t-d)} w_k \beta_k \Delta V_k \varphi_k(t+d) \sin(\theta_k) ] \cdot \vec{n}_n \\ \vec{Q}(t) = Q_p(t) \vec{n}_p + Q_n(t) \vec{n}_n \end{cases} \quad (16)$$

is the unit vector parallel to the reference  $n_p$  where

$n_n$  is the unit vector orthogonal to it.  $n_n$  vector and

The “Lead Field from Forward Problem” is the final part of the MEG modeling in Fig. 1. Electrical potential and magnetic field produced by activation in some voxels can be computed by quasi-static approximation of Maxwell equations [14]. After choosing a head model (spherical approximation or realistic head model), the following matrix equation relates the measured magnetic field and ECDs of voxels in the brain:

$$B(t) = L(\vec{r}_Q) \vec{Q}(t) \quad (17)$$

where  $\vec{Q}(t)$  is ECDs in region of interest in the brain,  $L$  is lead field matrix and  $B(t)$  is measured field by sensors.

### 3. Results

The proposed model contains several parameters whose values can be adjusted to reflect practical conditions. The effects of these parameters on the MEG and fMRI signals are analyzed and illustrated in this section. First, the nonlinear relation between synaptic activity and BOLD signal, reported in several papers, is shown. Then, a mathematical analysis of the model is presented to find the conditions under which there is a detectable BOLD signal in a voxel but the voxel is silent for MEG and vice versa. These conditions are verified and illustrated using simulation studies. Next, the difference between spatial responses of MEG and fMRI is shown.

#### 3.1. Nonlinearity Between Synaptic Activities and BOLD

It is generally accepted that the relation between stimulus and BOLD signal is nonlinear. This nonlinearity stems from stimulus to synaptic activities, from synaptic activity to CBF, and from CBF to BOLD. The relation between stimulus and synaptic activities has been reported to be nonlinear [31] but since the synaptic activities are input for both MEG and BOLD in our model, we do not focus on this relation. The relation between synaptic activities and CBF has been reported linear in some studies [13,31] and nonlinear in others [22,34]. The nonlinearity between CBF and BOLD is explained by the Balloon model and included in our model.

For evaluation of the nonlinearity in the proposed model, we consider impulse and step responses of synaptic activities according to block and event related stimuli in fMRI. The steady state (ss) response to the step function from (3)-(5) is derived from the following equations:

$$f_{in}^{ss} = 1 + \varepsilon u \tau_f \quad (18)$$

$$v^{ss} = (f_{in}^{ss})^\alpha, \quad q^{ss} = (1 - (1 - E_0)^{1/f_{in}^{ss}}) v^{ss} / E_0 \quad (19)$$

$$y(t) = V_0 \{ k_1 (1 - q^{ss}) + k_2 (1 - q^{ss} / v^{ss}) + k_3 (1 - v^{ss}) \} \quad (20)$$

where superscript “ss” shows the final value of each parameter after its steady state.  $u$  in (18) stands for synaptic activities. Although, the relation between CBF ( $f_{in}^{ss}$ ) and synaptic activities ( $u$ ) is linear in the proposed model as described by (18), the nonlinearity from synaptic activities to CBF can be modeled by considering a nonlinear function of  $u$  in (18). Two candidates for this nonlinear function are “sigmoid function” [34] and “inverse sigmoid function” [22]. The nonlinearity between CBF ( $f_{in}^{ss}$  in (19)) and BOLD ( $y(t)$  in (20)) makes our model nonlinear. The relation between synaptic activities and BOLD is depicted in Fig. 5 for both impulse and step responses and shows that BOLD is an increasing saturated function of synaptic activities. The nonlinear relationship between CBF and BOLD signal in this figure are related to the nonlinearity of the extended balloon model (due to Eqs. 18-20) which is in consistence with the experimental results [34,24].

#### 3.2. Exploring Relationship Between MEG and fMRI

Using the simulation results of the proposed model, we show that it is possible to detect the BOLD signal in a voxel while the voxel is silent for MEG and vice versa. Our model is based on Equations (1) to (17) as shown in Fig. 1. There are several parameters in the model, some of which are considered stochastic and others deterministic. In all simulations, the values for deterministic and pdfs for stochastic parameters are as described in the previous sections; any deviations from these values will be explained.

There are approximately  $10^5$  neurons per  $\text{mm}^3$  of cortex and thousands of synapses per neuron [15]. If the external stimulus causes activation in one percent of the synapses, then there are on the order of  $10^6$  active synapses in a voxel with the volume of  $1 \text{mm}^3$ . As mentioned in the previous section, the number of excitatory synapses generally is more than inhibitory synapses and we consider 10% for the ratio of IPSPs to all PSPs (we call this ratio as “IPSP ratio” hereafter). Fig. 6 shows simulation results in a voxel of  $1 \text{mm}^3$  with  $N_{ss} = 10^6$  active PSPs (according to (1)) and IPSP ratio of 10%. The stimulus duration is 1 second. The number of active PSPs (sum of EPSPs and IPSPs) during stimulation is depicted in Fig. 6-a. The current dipole produced by each PSP has an angle ( $\theta$ ) with the reference vector, in the  $[-\pi, \pi]$  range. Fig 6-b shows its pdf which is close to a uniform pdf.

The projected ECD to the reference vector ( $Q_p(t)$ ) and normal to this vector ( $Q_n(t)$ ) are depicted in Figs. 6-c and 6-d, respectively. According to (13) and the odd property of the sine function, the average value of ECD is

zero as shown in Fig. 6-d. Assuming the ECD peak value in the order of 10 nAm can be detected by the MEG sensors [15], the  $Q_p(t)$  in Fig. 6-c can be detected, although the pdf of  $\theta$  tends to a uniform pdf and it is expected that PSPs cancel each other. This is because the small difference between the pdf of  $\theta$  and uniform pdf is amplified by the huge number of active PSPs and thus detectable MEG signal is produced. The normalized synaptic activity is shown in Fig. 6-e and used as input to the extended Balloon model. Finally, Fig. 6-f shows the BOLD signal output of the model without considering

additive noise. The maximum contrast of the BOLD signal is 1.58%.

The simulation results in Fig. 7 show special cases where the BOLD signal is detectable but the MEG signal is not. There are two parameters in our model for this condition: the pdf of  $\theta$  and the IPSP ratio. When the pdf of  $\theta$  tends to uniform, then the directions of current dipoles are uniformly distributed and can cancel each other. Also, if

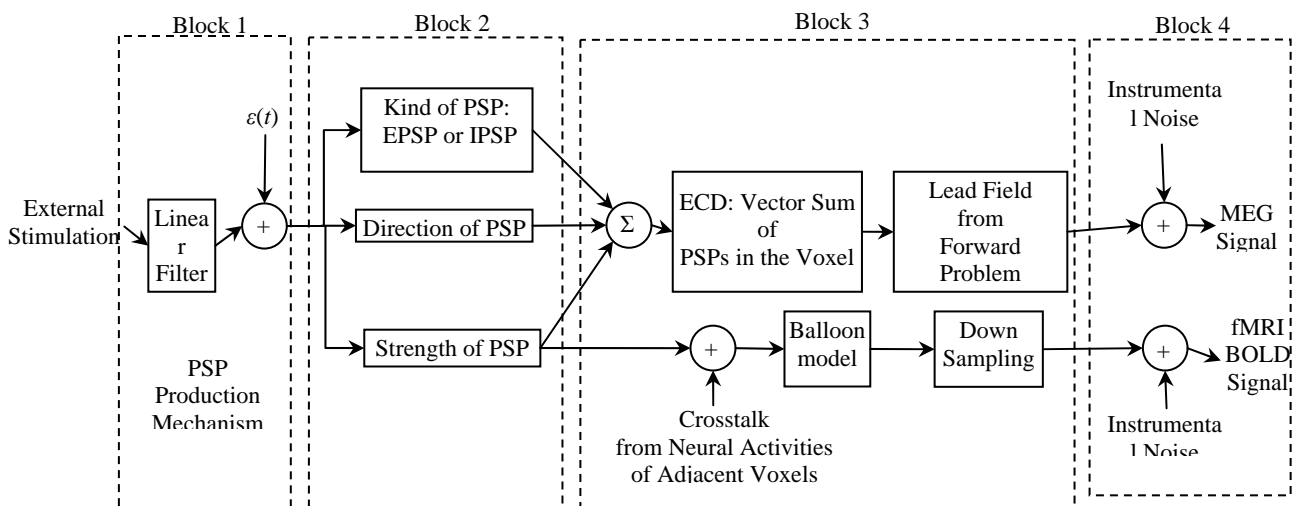


Fig. 1: Schematic Diagram for the proposed integrated MEG and Fmri model.



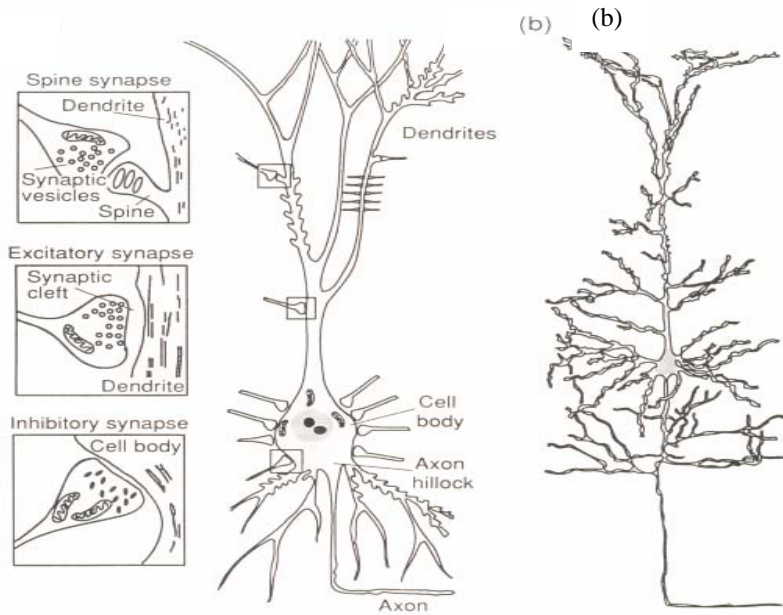


Fig. 2: Typical pyramidal neuron. (a) Schematic illustration of three magnified synapses. (b) Pyramidal neuron [15].

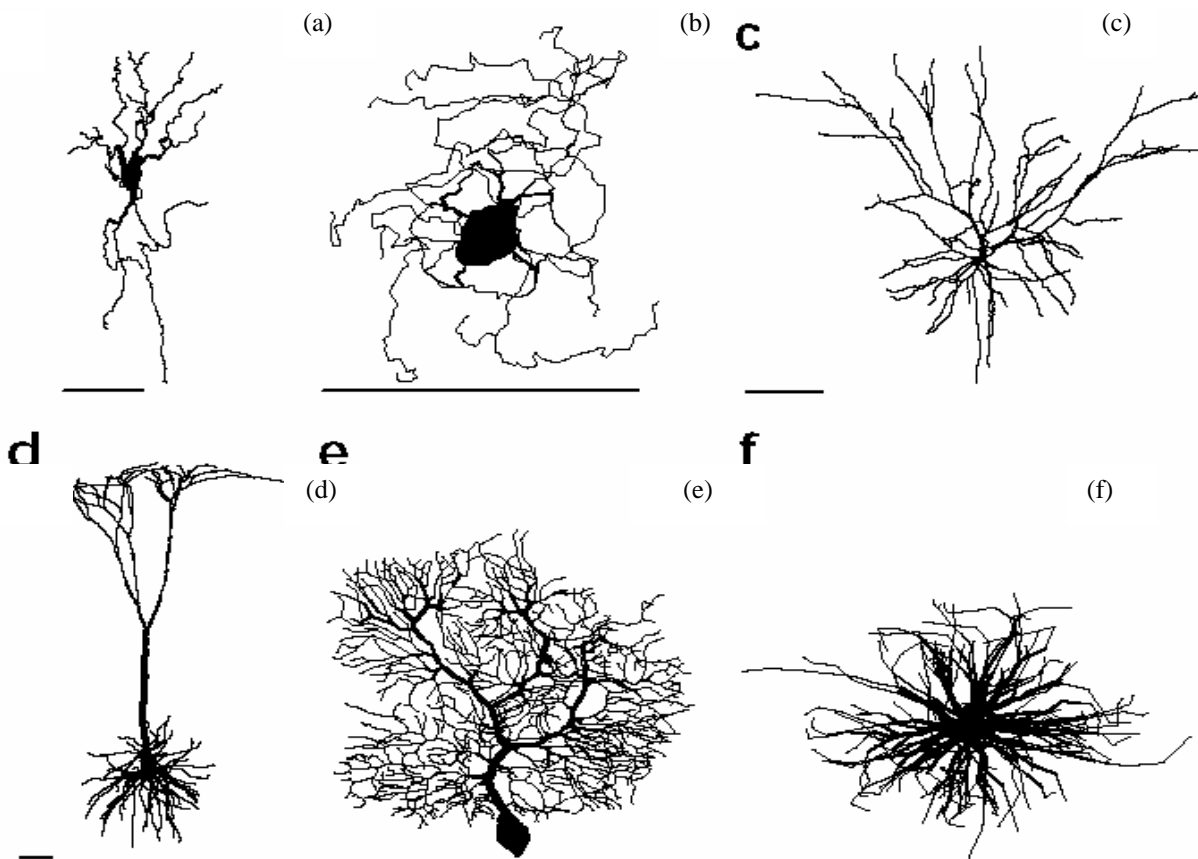


Fig. 3: Depending on the brain region, neurons with dendritic trees exist in all sorts of shapes and sizes. The dendritic trees for some kinds of neuron: (a) a vagal motoneuron; (b) an olivary neuron; (c) a layer 2/3 pyramidal cell; (d) a layer 5 pyramidal cell; (e) a Purkinje cell; and (f) an  $\alpha$ -motoneuron. Scale bars, 100  $\mu$ m [Segev, 1998].

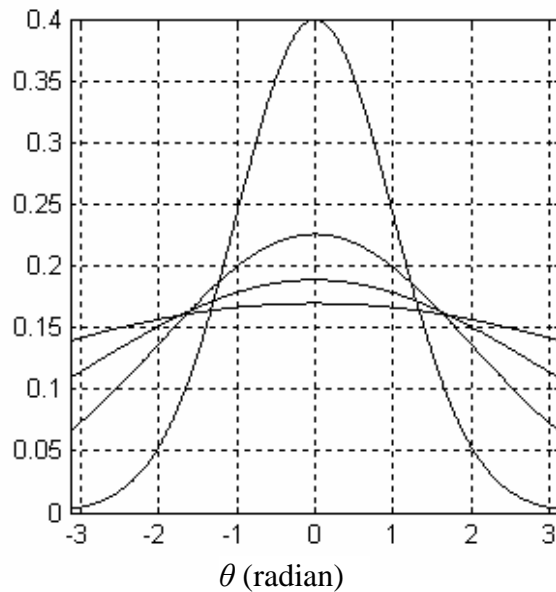


Fig. 4: pdf of  $\theta$  (angle between current dipole and reference vector) according to (13). The values of  $\sigma$  are 1, 2, 3 and 5 from maximum to minimum peak value of the 4 plotted functions.

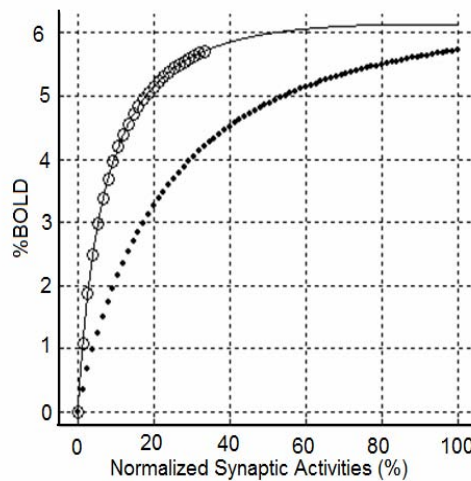
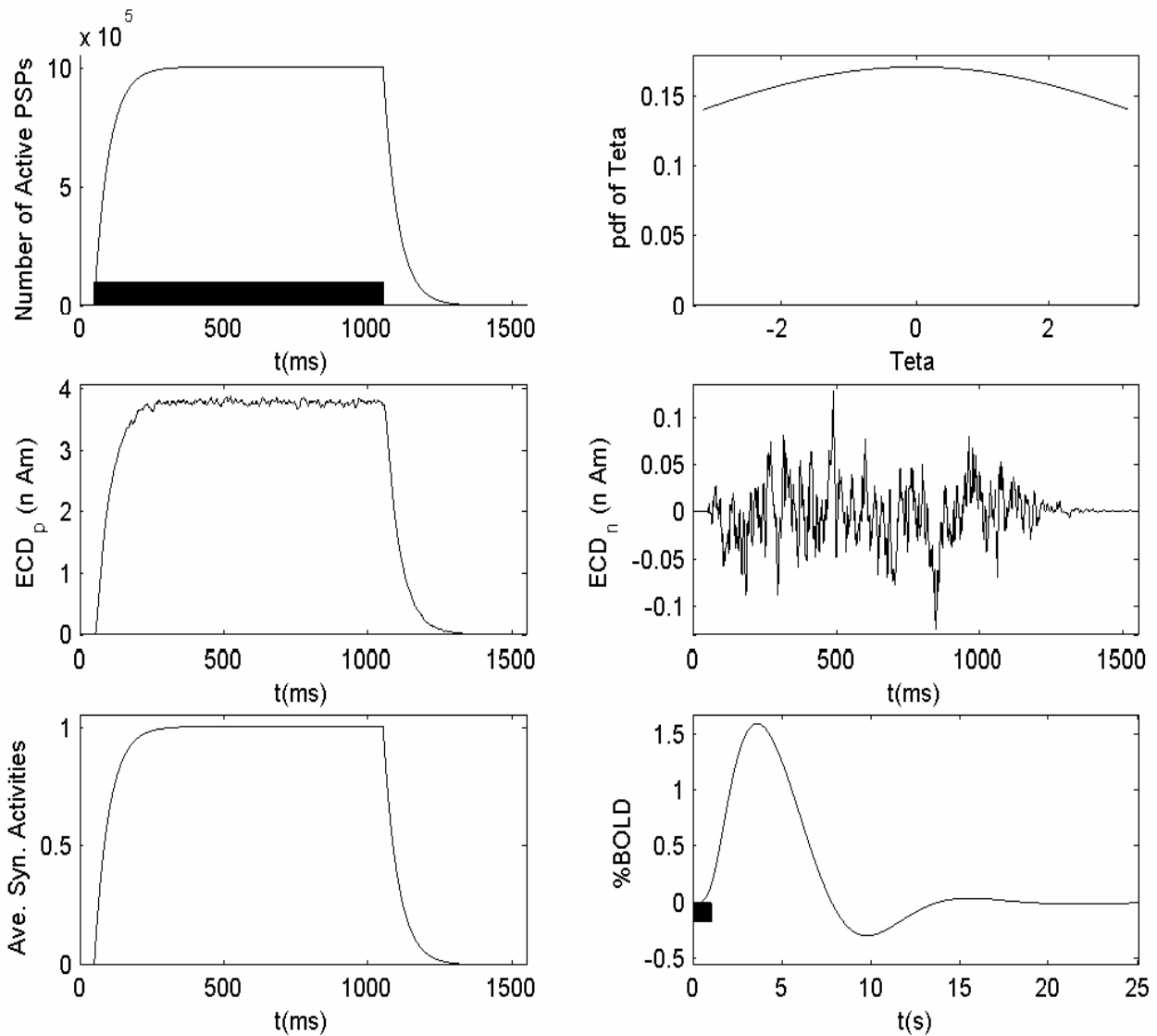


Fig. 5: Illustration of the nonlinear relationship between the BOLD signal and the normalized average synaptic activities. Solid line shows the step response of BOLD output from (18) – (20). ‘o’ plot shows the steady state solution values of the BOLD response with step input using “Simulink” toolbox in MATLAB for solving equations (3) – (5). The dotted plot is the same as ‘o’ for peak value of the impulse response.  $\alpha = 0.33$ ,  $E_0 = 0.34$  and  $V_0 = 0.02$  is considered in the Balloon model.



**Fig. 6: Illustration of the capability of the proposed model to generate both MEG and fMRI signals. The small black rectangle shows the duration of stimulation. (a) Number of active synapses according to (1) with  $\tau_d = 50$  ms. (b) pdf of  $\theta$  where  $\theta$  is the angle between PSP dipole and direction perpendicular to the cortical surface. (c) Projected ECD in the direction perpendicular to the cortical surface,  $Q_p(t)$  in (19). (d) Projected ECD in the direction tangent to the cortical surface,  $Q_n(t)$  in (19). (e) Average synaptic activity according to (9). (f) BOLD output according to (3)-(5).**

The numbers of IPSP and EPSP are equal (the IPSP ratio tends to 50%), they cancel each other because of opposite polarities. Since  $Q_p(t)$  is the only component correlated to the stimulation, it is the only component shown in Fig. 7. All conditions (except for the pdf of  $\theta$  and IPSP ratio) in Fig. 7 are the same as Fig. 6. Therefore, the BOLD output for all subplots of Fig. 7 will be the same as Fig. 6-f (not shown avoid repetitions) and so there will be detectable BOLD signal in all subplots.

The  $Q_p(t)$  for a conventional condition is shown in Fig. 7-a, where the pdf of  $\theta$  is the same as that in Fig. 6-b and the IPSP ratio is 10%. The best condition for detecting MEG is shown in Fig. 7-b, where all current dipoles are considered parallel ( $f_\theta(\theta) = \delta(\theta)$  in (13)) and also all PSPs are considered EPSPs without any IPSP (IPSP ratio is zero). The amplitude of ECD in this condition is about 30 times larger than that of Fig. 7-a. The pdf of  $\theta$  is considered to be uniform and the IPSP ratio is set to 10% in Fig. 7-c. In Fig. 7-d, the IPSP ratio is set to zero and the pdf of  $\theta$  is the same as that of Fig. 6-b. The ECD in both Figs. 7-c and 7-d is like random noise with zero mean and so there is no detectable MEG signal correlated with the stimulus, although there are detectable BOLD signals for both figures.

Since 2/3 of neurons in gray matter are pyramidal cells [35], we expect the pdf of  $\theta$  be similar to Fig. 6-b or even more concentrated around zero. Also, in most neurons, the IPSP ratio is less than 20% [14,31], thus Fig. 6-a shows a real condition for many regions of the brain. However, in some regions like cerebellum (that contains Purkinje cells) the pdf of  $\theta$  tends to uniform and we expect conditions like Fig. 7-c for MEG signal from this region. Although the number of excitatory synapses is more than inhibitory synapses in most neurons, there are some neurons with considerable number of inhibitory synapses compared to excitatory synapses [14] and so conditions like Fig. 7-d is also possible.

Now, we intend to quantitatively evaluate effects of pdf of  $\theta$  and IPSP ratio on MEG and fMRI signals. After the number of active synapses reaches its final steady state value according to (1), the number of active synapses becomes almost fixed. Referring to (16), we have:

$$\bar{Q} = \left[ \sum_{d=0}^D \sum_{k=1}^N w_k \beta_k \Delta V_k \varphi_k(d) \cos(\theta_k) \right] \cdot \bar{n}_p + \left[ \sum_{d=0}^D \sum_{k=1}^N w_k \beta_k \Delta V_k \varphi_k(d) \sin(\theta_k) \right] \cdot \bar{n}_n \quad (21)$$

where  $N$  is the average number of active synapses after steady state. If all random variables in (21) are considered independent, the mean value of ECD is:

$$\bar{Q} = \left\{ \sum_{d=0}^D \sum_{k=1}^N E[w_k] E[\beta_k] E[\Delta V_k] E[\varphi_k(d)] E[\cos(\theta_k)] \right\} \cdot \bar{n}_p = \bar{Q} \cdot \bar{n}_p \quad (22)$$

$$\bar{Q} = \bar{\varphi} \bar{V} \bar{\beta} N (1 - 2r) g(\sigma_\theta) \quad (23)$$

where  $E[.]$  is "expected value",  $r$  is the mean value of IPSP ratio,  $\bar{V}$  is mean amplitude of PSP,  $\bar{\beta}$  is mean of  $\beta$  according to (12),  $\bar{\varphi} = \sum_{d=0}^D E[\varphi_k(d)]$  according to

$\varphi(t)$  in (6) with  $\tau_{PSP} \sim TN(2,1; 0, \infty)$  ms and  $g(\sigma_\theta)$  shows average effects of projected ECD onto the reference vector. The second term of (21) vanishes in averaging because of odd property of the sine function and even property of the pdf of  $\theta$ . The  $g(\sigma_\theta)$  is defined by:

$$\cos(\theta) \frac{e^{-\frac{\theta^2}{2\sigma^2}}}{k} d\theta \quad ; \quad k = \sqrt{2\pi} \sigma \operatorname{erf}\left(\frac{\pi}{\sqrt{2}\sigma}\right) \quad (24)$$

$$-2 \left(1 - \frac{2\pi\sigma^2}{k} e^{-\frac{\pi^2}{2\sigma^2}}\right)$$

where  $\sigma_\theta$  is the standard deviation of  $\theta$ . It is plotted versus  $\sigma$  and  $\sigma_\theta$  in Fig. 8. When  $\sigma \rightarrow 0$ , then  $\sigma_\theta \rightarrow 0$  and the pdf of  $\theta$  is like the Dirac delta function and  $g(\sigma_\theta) \rightarrow 1$ . When  $\sigma \rightarrow \infty$ , then  $\sigma_\theta \rightarrow \pi^2/3$  and the pdf of  $\theta$  is uniform and  $g(\sigma_\theta) \rightarrow 0$ .

The synaptic activities in fMRI are derived from (10):

$$\begin{cases} \bar{u} \propto E\left[\sum_{k=1}^N \tau_{PSP}^k \Delta V_k\right] \\ \bar{u} \propto N \bar{\tau}_{PSP} \bar{V} \Rightarrow \bar{u} = u_m \frac{N}{\max(N)} \end{cases} \quad (25)$$

where  $u_m$  is the synaptic activity that produces the saturated maximum output in the extended Balloon model and  $\max(N)$  shows the maximum number of PSPs in a voxel that can be activated by an external stimulus.

Inserting (25) in (23), we have:

$$\begin{cases} \bar{Q} = \bar{\varphi} \bar{V} \bar{\beta} \max(N) (1 - 2r) g(\sigma_\theta) \frac{\bar{u}}{u_m} \\ \bar{Q} = \bar{Q}_m (1 - 2r) g(\sigma_\theta) \frac{\bar{u}}{u_m} \end{cases} \quad (26)$$

Considering (3)-(5) in the extended Balloon model and (26), the relation between BOLD signal and ECD is:

$$\begin{cases} \bar{Q} = \bar{Q}_m (1 - 2r) g(\sigma_\theta) \frac{\bar{u}}{u_m} \\ \text{BOLD Output} = \text{Balloon Model}(\bar{u}) \end{cases} \quad (27)$$

The relations between ECD ( $\bar{Q}$ ) in MEG, average synaptic activities ( $\bar{u}$ ), and BOLD output in fMRI are

summarized in (27). This equation shows that the relation between ECD and BOLD is nonlinear and segregates to two parts: linear relation between ECD and  $\bar{u}$  and nonlinear relation between BOLD and  $\bar{u}$  according to the nonlinearity of the Balloon model.

Fig. 9 illustrates the relation between ECD and BOLD. Fig. 9-a shows this relation according to (27) with  $r = 0$  and  $\sigma_\theta = 0$  ( $g(\sigma_\theta) = 1$ ) where BOLD increases as ECD moment increases with an increasing saturated function. This function can be separated to three regions. For increasing ECD from zero to 1%, the BOLD contrast is less than 15% of its maximum. The ECD and BOLD signals are very small and cannot be detected in this region of the curve. The second part contains the steepest part of the curve for the BOLD signal, where increasing ECD from 1% to 27% increases BOLD from 15% to 90%. The BOLD signal is saturated in the third part where 73% increase in ECD increases BOLD signal by only 10%. As illustrated in Fig. 5, the nonlinear relationship between the neural activity and the BOLD signal (which is reported in experimental results [Nielsen and Lauritzen, 2001; Lauritzen and Gold, 2003]) can be generated in the proposed model. We expect nonlinear relationship between the ECD and the BOLD signal according to the linear relationship between the neural activity and the ECD (as we assumed in the model) and nonlinear relationship between the neural activity and the BOLD signal. The figs. 5 and 9 are actually similar if the plot in fig. 5 is considered as logarithmic plot.

Effects of pdf of  $\theta$  on ECD and BOLD signals are shown in Fig. 9-b. Three curves are plotted for  $\sigma = 0, 10$  and  $25$  with  $r = 0$  for all curves. Fig 9-b shows that for a high value of  $\sigma = 25$  (pdf of  $\theta$  tends to uniform) even though the BOLD signal is saturated at its maximum value, the ECD is less than 0.2% of its maximum and is not detectable. Effects of IPSP ratio ( $r$ ) on ECD and BOLD are shown in Fig. 9-c for three values of IPSP ratio,  $r = 0, 20\%$  and  $40\%$  and  $\sigma = 0$  for all curves. When  $r$  tends to 50% (canceling EPSPs with IPSPs), the ECD tends to zero although the BOLD signal is detectable at its maximum value. For a 1.5 T scanner and  $TE = 40$  ms, parameters  $k_1, k_2,$  and  $k_3$  in equation (20) have been evaluated to be  $k_1 = 7E_0, k_2 = 2,$  and  $k_3 = 2E_0 \cdot 0.2$  in [7]. The maximum BOLD contrast in this condition is about 6% which is shown in Fig. 9.

We assume a detectable signal in each case of ECD or BOLD and show effects of  $\sigma$  (pdf of  $\theta$ ) and  $r$  (IPSP ratio) on the detection of the other one in Fig. 10. The BOLD contrast is fixed at 2% in Figs. 10-a and 10-b and the resulting ECD is plotted as functions of  $\sigma$  and  $r$ . Note that increasing  $\sigma$  and  $r$  decreases ECD to zero and thus even though the BOLD signal is detectable, there may be no detectable MEG signal. In Figs. 10-c and 10-d, the value of ECD is set to a detectable level (10% of its

maximum) and the resultant BOLD contrast is plotted as functions of  $\sigma$  and  $r$ . Note that with even very low value of ECD, increasing  $\sigma$  and  $r$  may increase the BOLD contrast to its maximum saturation value.

### 3.3. Spatial Response of MEG and fMRI

The neural activities in each voxel are independent of other voxels in the proposed model and therefore there is no crosstalk between ECDs. However, the non-uniqueness property of the "Inverse Problem" in MEG may cause some voxels without neural activity to show activity in the solution of linear equation (17) [26], which we call "crosstalk." On the other hand, neural activities in a voxel can change CBF and BOLD signal in the neighboring voxels and cause false detection of activity in these voxels, as discussed in Section II-B-2 and considered in our proposed model (Fig. 1). Accordingly, in the spatial response of each method, it is possible that some voxels are detected as active without containing any neural activity, and so the spatial response of the two modalities may be different.

Fig. 11 illustrates the effect of spatial crosstalk in fMRI. All parameters for producing simulated data are the same as the first simulation in Section III-B and Fig. 6. One of the middle axial slices of MRI is used as the base image. The region of interest is limited to a window with the size of  $64 \times 64$  voxels (pixels) where a pixel in the center of the window is the single active pixel (Fig. 11-a). The pixel size is  $0.75 \times 0.75 \text{ mm}^2$  and is selected smaller than its conventional value to manifest the effect of spatial blurring. The average synaptic activities and the BOLD output in this pixel are shown in Fig. 6-e and Fig. 6-f, respectively. Fig. 11-b shows BOLD signal after down sampling with  $TR = 2$  sec.

For modeling the crosstalk effect, we use (2) with 2D Gaussian distribution for  $G$  and  $\sigma_x = \sigma_y = \sigma = 1.5 \text{ mm}$ , i.e.,

$$G(x, y) = \frac{1}{2\pi\sigma^2} e^{-\frac{(x-x_0)^2 + (y-y_0)^2}{2\sigma^2}}; \quad (28)$$

where  $(x_0, y_0) = (32, 32)$  shows a central pixel of the image that is the single active pixel. The induced a

is used as the input of the Balloon model, whose output is the BOLD signal of each pixel. Duration of stimulus is 1 sec and each period of BOLD signal contains 12 samples ( $12 \cdot 2 = 24$  sec)

The data is repeated for 20 periods and so the total number of samples in each pixel is  $12 \times 20 = 240$ . Additive Gaussian white noise is added to all pixels so that the contrast to noise is 1. We use the “cross-correlation method” for activation detection. For the reference waveform in this method, we first calculate the impulse response of the Balloon model for an average neural activity, then construct the reference waveform by convolving stimulus pulse and the calculated impulse response. The false alarm rate is set to 1%.

The detected active pixels are shown in Fig. 11-c. Except 4 falsely detected pixels on the periphery of the image, the other detected pixels concentrate around the center of the image where we put the single active pixel. The number of active pixels is 25 and maximum distance between the detected pixels and the center is 3 pixels (2.25 mm). As the number of periods and the contrast to noise increase, the number of active pixels and activation radius will also increase. This simulation shows the possibility of detecting false activations adjacent to the active pixels in fMRI BOLD analysis.

Now, we deal with the effect of inverse problem on spatial response of MEG. The Minimum Norm (MN) method is used for solving the inverse problem according to the forward problem in (17) as [42]:

$$\begin{cases} \mathbf{B}(t) = \mathbf{L} \mathbf{Q}(t) \\ \hat{\mathbf{Q}}(t) = \mathbf{L}^\# \mathbf{B}(t) \end{cases} \quad (29)$$

where  $\mathbf{Q}$  is the current dipole moment in each voxel in the region of interest,  $\mathbf{L}$  is lead field matrix,  $\mathbf{B}$  is detected signal in the MEG sensors,  $\mathbf{L}^\#$  is pseudo-inverse of  $\mathbf{L}$ , and  $\hat{\mathbf{Q}}$  is MN solution for estimated current dipole. We used the coordinate of BTi Magnes 2500WHS neuromagnetometer system with 147 active magnetometer detectors in our simulation. A volumetric structural MRI data of head with  $314 \times 256 \times 256$  voxels and volume of each voxel approximately  $0.75 \times 0.75 \times 0.75 \text{ mm}^3$  is used for co-registration. The solution is considered at representative axial slice of the MRI (Fig. 12-c) and the region of interest is restricted to only gray matter with 17,970 pixels as shown in Fig. 12-a. Active region contains only one pixel whose current dipole is perpendicular to the cortical surface (Fig. 12-a). Fig. 12-b shows the MN solution for the moment of the current dipole. The direction of maximum moment in the solution space is shown in Fig. 12-c.

The simulation results of 3D whole head model are shown in Fig. 13. Thirty-three axial slices of MRI are considered which contain cortical voxels. The volume contains  $64 \times 79 \times 33$  voxels of size  $3 \times 3 \times 3 \text{ mm}^3$  (Fig 13-a). Only 1 voxel is considered as active voxel whose location is shown in Fig. 13-a. The region of interest in MEG is limited to 24,271 voxels of gray mater. The direction of ECD in the active voxel and the MN solution are shown in Fig. 13-a. The voxel size in the fMRI simulation is considered as  $0.75 \times 0.75 \times 0.75 \text{ mm}^3$  for enhanced observation of spatial blurring. The 3D

Gaussian distribution for  $G$  is considered in (2) with  $\sigma_x = \sigma_y = 2.6 \text{ mm}$  and  $\sigma_z = 0.7 \text{ mm}$  where the  $x$ - $y$  plane is parallel and  $z$  axis is perpendicular to the axial slice. The false alarm rate and contrast to noise ratio are set to 0.1% and 0.2, respectively. The other parameters of neural activities related to this single active voxel are the same as the previous simulation in Fig. 11. The spatial blurring in fMRI response and spread of the MN solution of MEG are shown in Fig. 13.

In summary, neural activity in a voxel can produce BOLD signal in the neighboring voxels and cause blurring in the spatial response of the fMRI. Also, the non-uniqueness property of the MEG inverse problem spreads the solution to a wide region. Therefore, if there are neural activity in a voxel that produce detectable ECD and BOLD signal, the spatial response of fMRI and MEG are not necessarily the same.

#### 4. Estimation of the Parameters Using Real Data

For validation of the proposed model in real conditions, we use real auditory MEG and fMRI datasets from 2 normal subjects to estimate the parameters of the model. Details of our work can be found in [5]. However, we try to summarize the methods and results in this section.

##### 4.1. Auditory Task Data

Parameters of the proposed model are estimated using real datasets of auditory block stimulus from two healthy male and female subjects. Each block consists of 12 seconds of *tones on* followed by 12 seconds of *tones off*. During the *tones on* period, 3 tone bursts presented with a 15 ms rise/fall time at a rate of one per second for each of 4 tone frequencies 500Hz, 750 Hz, 1000 Hz, and 1200 Hz as illustrated in Fig. 14.

The MEG datasets gather using 148 channel whole head Neuromagnetometer (4D Neuroimaging). 50 blocks (epochs) of MEG data are acquired with sample rate of 508.63 Hz. The heart artifact is removed and the datasets are filtered using a band-pass filter (0.5 Hz to 50 Hz) before analysis. The MEG signal of the male subject (subject # 1) is illustrated in Fig. 15. For this subject, the 78th sensor (near to the primary auditory cortex) has most significant signal compared to other sensors. The average signal of this sensor over all 50 epochs is illustrated in Fig. 15-a. We used independent component analysis (ICA) on the raw data (before averaging over 50 epochs) as the next preprocessing stage after discarding the nuisance channels. Then, the averaged ICA component over all epochs is calculated. The stimulus correlated component of ICA is illustrated in Fig. 15-b. The contour map of this component in all sensors is shown in Fig. 16.

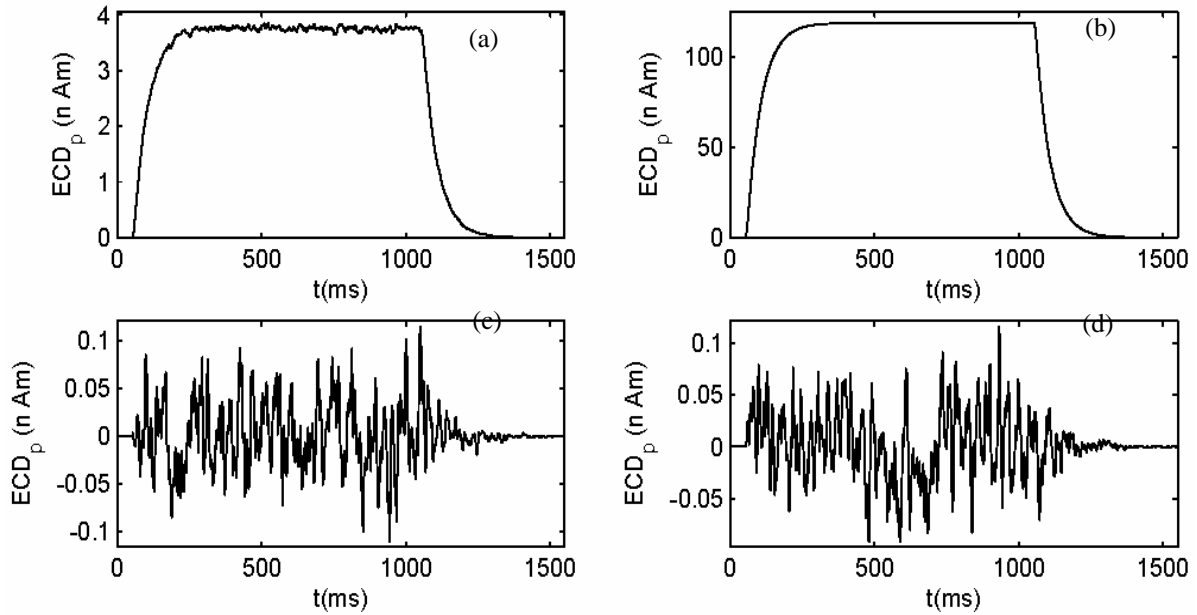


Fig. 7: Illustration of cases that MEG signal is significant or small, using the effects of pdf of  $\theta$  and ratio of IPSPs number to all PSPs on ECD ( $Q_p(t)$ ) in MEG signals. (a) pdf of  $\theta$  is same as Fig. 6-b and IPSP ratio is set to 10%. (b)  $f_\theta(\theta) = \delta(\theta)$  and IPSP ratio is set to zero. (c) pdf  $\theta$  is set to uniform distribution around  $[-\pi, \pi]$  and IPSP ratio is set to 10%. (d) pdf  $\theta$  is same as Fig. 6-b and IPSP ratio is set to 50%

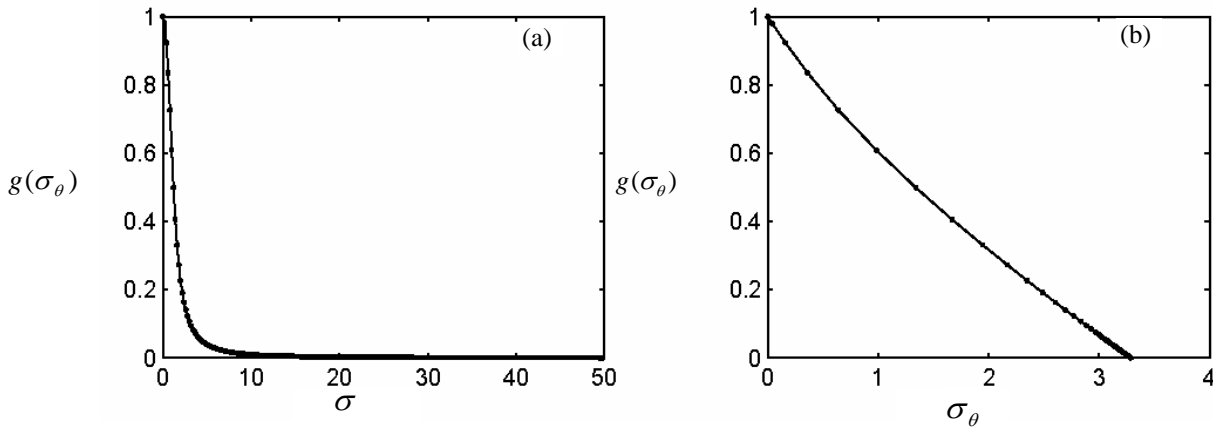
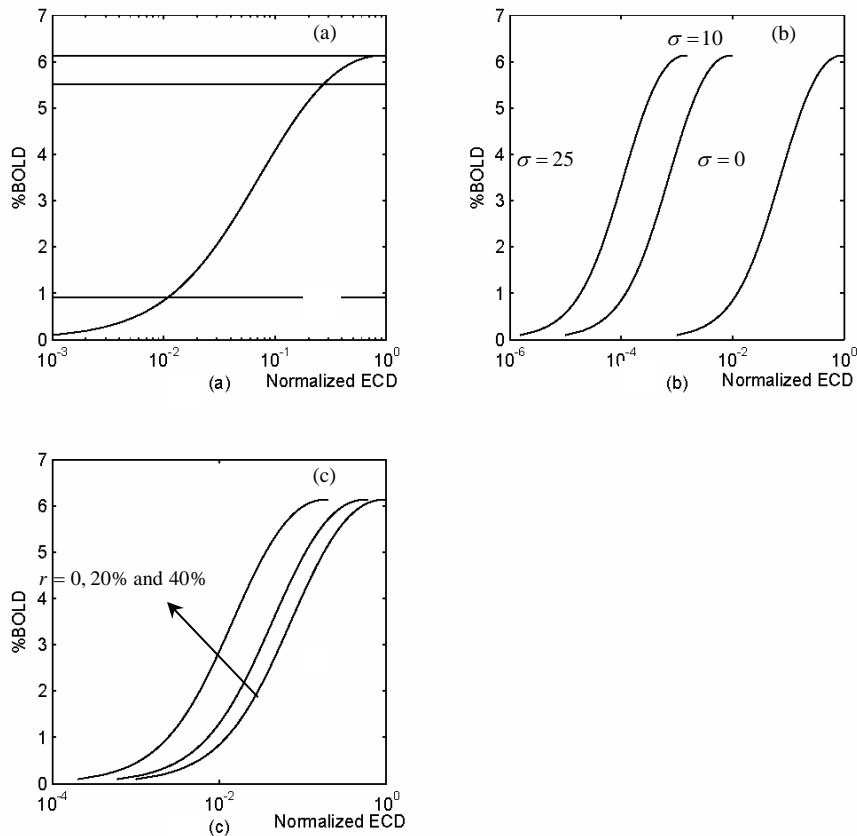
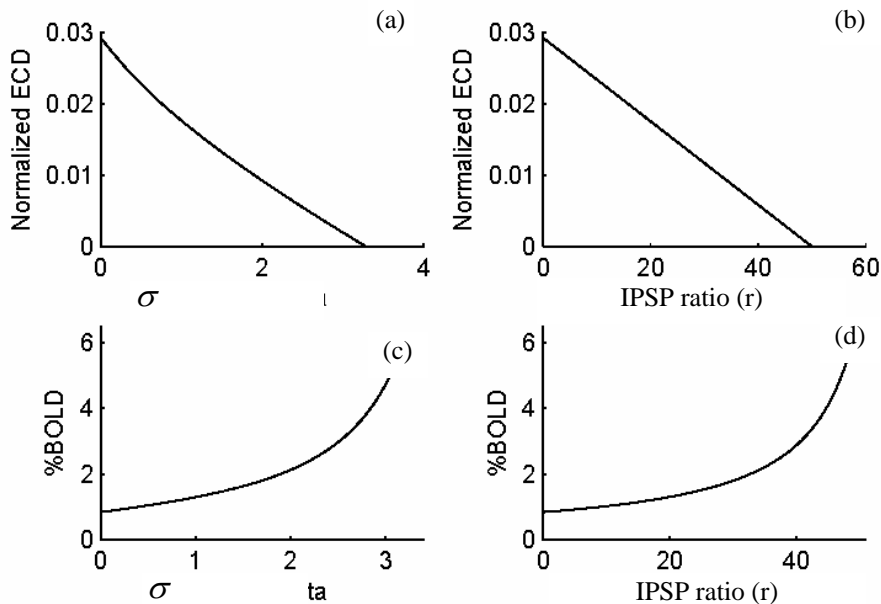


Fig. 8: Illustration of the nonlinear function that relates the standard deviation of  $\theta$  to ECD according to (24). (a)  $g(\sigma_\theta)$  versus  $\sigma$ . (b)  $g(\sigma_\theta)$  versus  $\sigma_\theta$ .



**Fig. 9:** Illustration of the effects of two parameters (standard deviation of theta and ratio of IPSP to all PSP) on the MEG and fMRI signals. Relation between ECD and BOLD according to (31) for: (a)  $r = 0$  and  $\sigma = 0$  ( $g(\sigma_\theta) = 1$ ). The horizontal lines show 15%, 90% and 100% of maximum BOLD signal. (b)  $r = 0$  and  $\sigma = 0, 10$  and  $25$ . (c)  $\sigma = 0$  and  $r = 0, 20\%$  and  $40\%$ .



**Fig. 10:** Illustration of the conditions where detectable fMRI signal is considered but MEG signal changes as a function of  $\sigma$  (pdf of  $\theta$ ) and  $r$  (IPSP ratio) and vice versa. (a) Contrast of BOLD is fixed at 2% and  $r = 0$ . (b) Contrast of BOLD is fixed at 2% and  $\sigma = 0$ . (c) Value of ECD is fixed at 10% of its maximum value and  $r = 0$ . (d) Value of ECD is fixed at 10% of its maximum value and  $\sigma = 0$ .



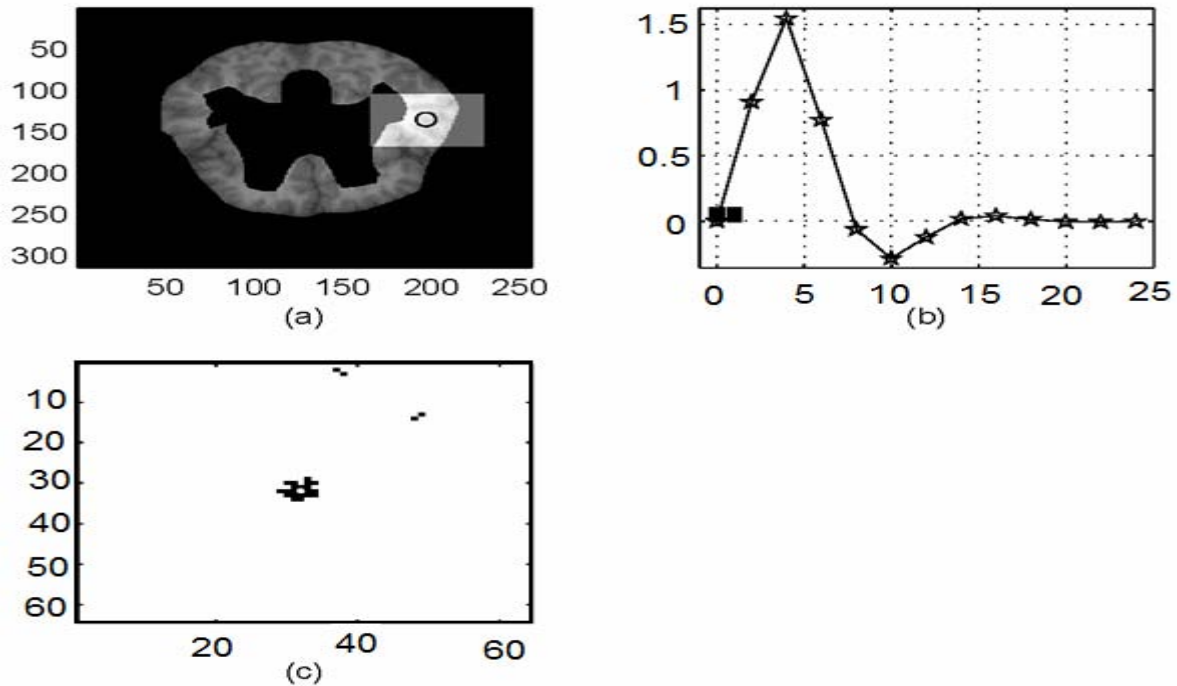


Fig. 11: Illustration of the effect of spatial crosstalk on the fMRI response. All parameters are the same as Fig. 6. (a) The region of interest is limited to a window with  $64 \times 64$  pixels and the location of active pixel is shown by circle. (b) One period of BOLD output from the Balloon model with neural activities of Fig. 6-e. The small black rectangle shows the duration of stimulation. (c) The black pixels are detected active pixels. The white pixel at the center of the image shows the location of neural activities. The pixel size is  $0.75 \times 0.75 \text{ mm}^2$  and  $\sigma_x = \sigma_y = \sigma = 1.5 \text{ mm}$  according to (32).

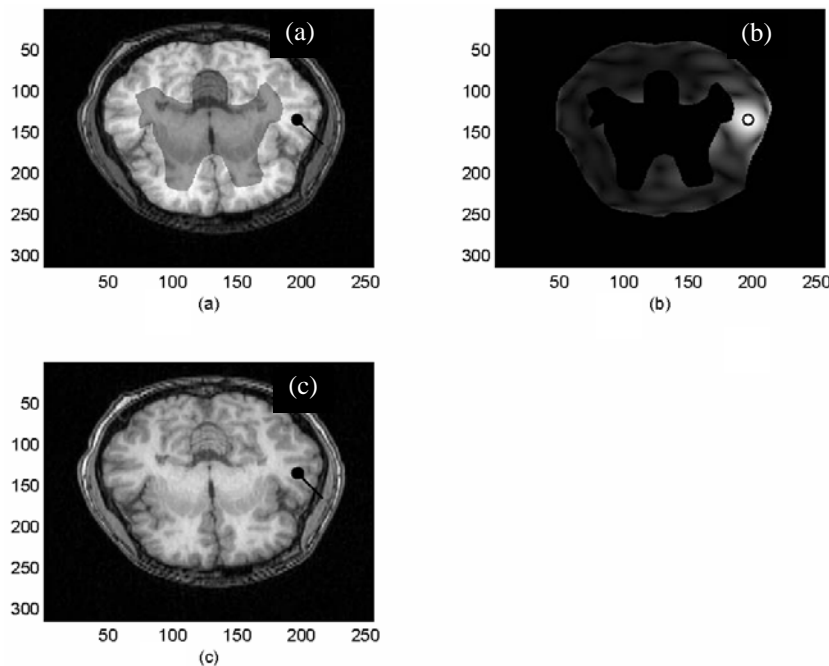


Fig. 12: Solution of Minimum Norm (MN) for MEG inverse problem. (a) The middle axial slice of MRI used for region of interest (ROI). The ROI is limited to general regions of gray matter shown with higher brightness. The source is current dipole in a single pixel. Its direction is perpendicular to the cortical surface. (b) Solution of MN where brightness reflects strength of dipoles. Location of source is shown by circle. (c) The location and direction of maximum moment dipole in the solution space.

The resolution of the 3-D anatomical MRI data is 256x256x66 voxels where the voxel size is 0.9375x0.9375x2.5 mm<sup>3</sup>. We use MEG-Tools (<http://www.megimaging.com/>) for coregistration of the MEG data with the 3-D anatomical MRI data. The MEG localizations are computed in reference to the Cartesian coordinate system defined by a set of three anatomical landmarks (fiducial points): the right and left external meatus or pre auricular and nasion. Prior to the MEG scan, the head surface is digitized using laser fast track scanning. The head digitization points (about 3,000 points) are used to ensure a precise registration, when the points laid on the scalp surface of the MRI scan.

For the fMRI studies, we use the GE product echo planner imaging (EPI) sequence with 64 by 64 data acquisition matrix, TE of 30 ms, TR of 2 s, field of view of 240 mm, and slice thickness of 5 mm. Each volume contains 16 slices. After discarding first few volumes, 16 block sequences of the fMRI data are acquired using the same MEG stimulus. Auditory stimulus is presented through air conductance tubes to headphones to reduce external noise. Motion is corrected using the statistical parametric mapping (SPM) and then the linear drift is removed from the data. We use the t-test [2] for activation detection and assume a simple linear model for the hemodynamic response function. SPM is used for the registration of the detected activation in the fMRI slices to the 3D anatomical MRI data.

#### 4.2. MEG Parameters Estimation

After registering the MEG coordinates to the 3D anatomical MRI data, the cortical model is constructed using 2,734 cortical locations in the subjects' gray matters. The concentric spherical head model is used to construct the forward model in (17). We use the stimulus correlated component of ICA for activation detection in MEG and we call this component as "main ICA component" hereafter. If main ICA component is considered as the MEG signal in all sensors, the time course of each sensor will be equal to the time course of this component multiplied by a scalar. The spatial pattern of the ICA component is the values of this scalar in all sensors. The temporal and spatial patterns of the main ICA component for subject # 1 are shown in Figs. 15-b and 16, respectively.

The Multi-Resolution FOCUSS (MR-FOCUSS) [23] is used to solve the MEG inverse problem and activation detection. The relationship between the dipoles and the measured field by the sensors is linear according to (29). Thus, the time courses of the activation in all cortical voxels are similar to the time course of the main ICA component and the differences between them are the magnitude and direction of the current dipole in each voxel. Assuming known pdfs for all random variables, we have the following equation according to Eq. (23):

$$\bar{Q}(t) = K_M \cdot N(t) \quad (30)$$

where  $K_M$  is a spatial parameter that represents the mean of all random variables in (23).

According to (30), the spatial and temporal parts of ECD in each voxel can be separated into two parts:  $K_M$  and  $N(t)$ .  $N(t)$  can be assumed proportional to the waveform of the main ICA component. Moreover,  $K_M$  in each voxel is the magnitude of the dipole calculated by the inverse solution of the scalar map shown in Fig. 16.

After assuming the main ICA component as  $N(t)$ , parameters of the linear filter in (1) can be estimated. For both subjects, we found that a first order linear filter according to (1) generates reasonable estimation results. Thus, we use the following first order linear filter.

$$T_p \frac{dN(t)}{dt} + N(t) = K \text{Stm}(t - T_d) \quad (31)$$

where  $T_p$ ,  $T_d$ , and  $K$  are parameters to be estimated and  $N(t)$  is the main ICA component. We estimate the parameters of this linear filter using the stimulus profile shown in Fig. 14 and assuming  $N(t)$  as the calculated main ICA component. For estimating these parameters, we used "fminsearch" function of the MATLAB which is an iterative method for finding the minimum of the mean square error between  $N(t)$  and its estimation according to (31).  $N(t)$  and its estimation for subject # 1 are shown in Fig. 15-d. The estimated values of  $T_p$ ,  $T_d$ , and  $K$  for both subjects are given in Table 1.

#### 4.3. fMRI Parameters Estimation

The parameters of the proposed model which are related to the fMRI part of the model can be partitioned into two sets: parameters related to the spatial crosstalk in (2); and parameters of the EBM according to Eqs. (18)-(20). At First, we estimate the parameters related to the spatial crosstalk. The detected activation from the fMRI data of subject # 2 co-registered to 3-D anatomical MRI is illustrated in Fig. 17.

For estimating the spatial crosstalk represented by  $\sigma = (\sigma_x, \sigma_y, \sigma_z)$  in Eq. (2), two Gaussian kernels are fitted to the main clusters of the detected activation areas in left and right primary auditory cortices. The hotspot of the cluster is assumed as the center of the Gaussian kernel. All neighboring voxels to the central voxel in a sphere with a diameter of 25 mm are considered for curve fitting. The estimated  $\sigma$  is given in Table 1.

For estimating the parameters of the EBM, we use average BOLD responses over 16 blocks of all active voxels for both subjects. We try to fit an EBM to average BOLD response of each voxel by estimating the parameters of the EBM. The parameters of the linear filter in Eq. (31) are estimated using the MEG

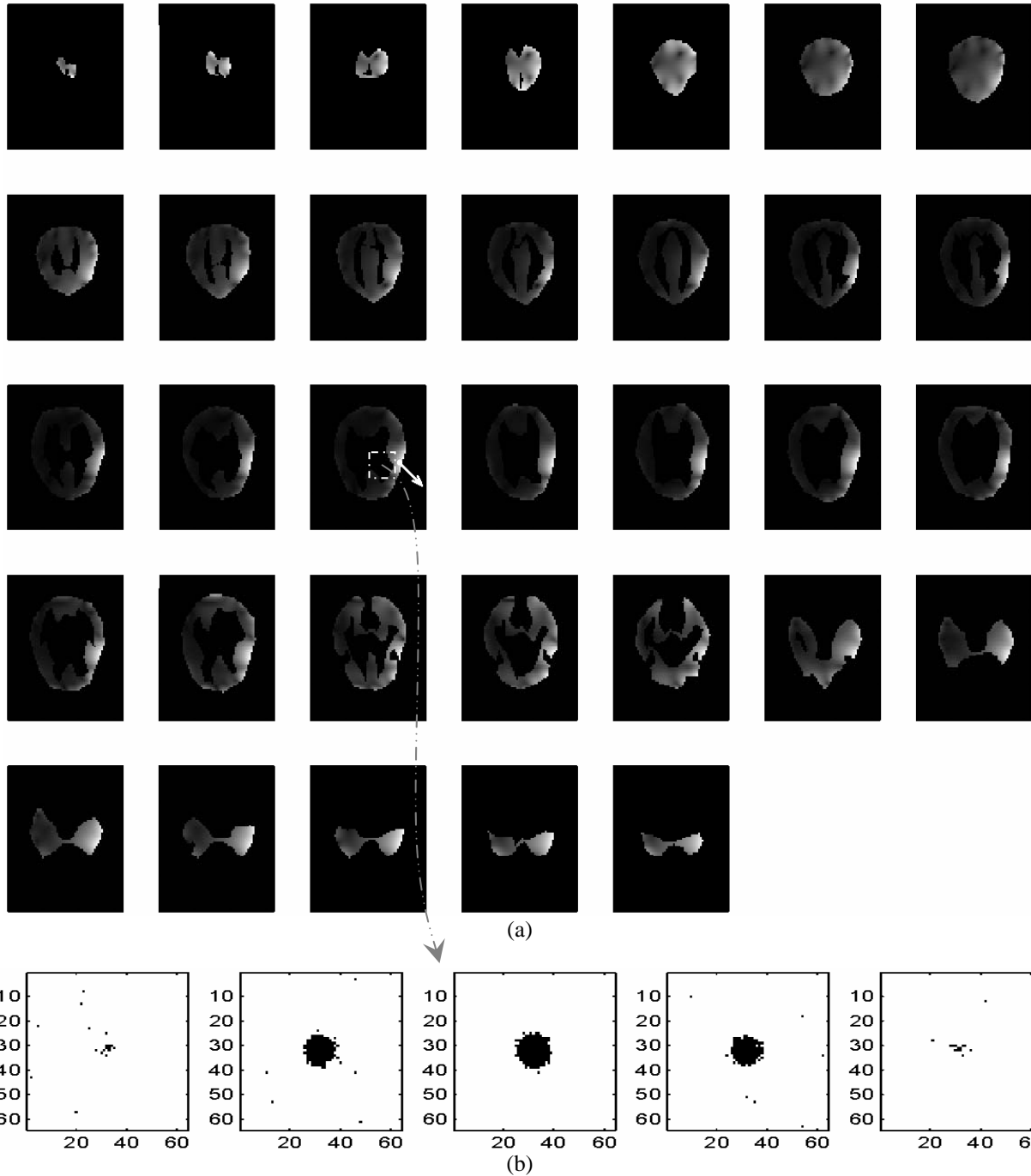


**Fig. 13:** Simulation in 3D whole head model for observing the difference in spatial responses of fMRI and MEG. (a) MN solution of inverse problem in MEG where brightness reflects strength of dipoles. The volume contains 33 axial slices and the voxel size is  $3 \times 3 \times 3 \text{ mm}^3$ . The region of interest is limited to 24,271 voxels of gray matter in the MN solution. The source is only 1 active voxel as single ECD whose location and direction is shown. (b) fMRI detected activation. The active voxel is the central voxel in the middle slice of the 5 axial slices. Voxel size is  $0.75 \times 0.75 \times 0.75 \text{ mm}^3$ . Note that the fMRI response is limited to a focused area of an ellipsoid with radii of 11mm and 1.5 mm but the MEG response is spread in all slices on the brain with wide regions in each slice.

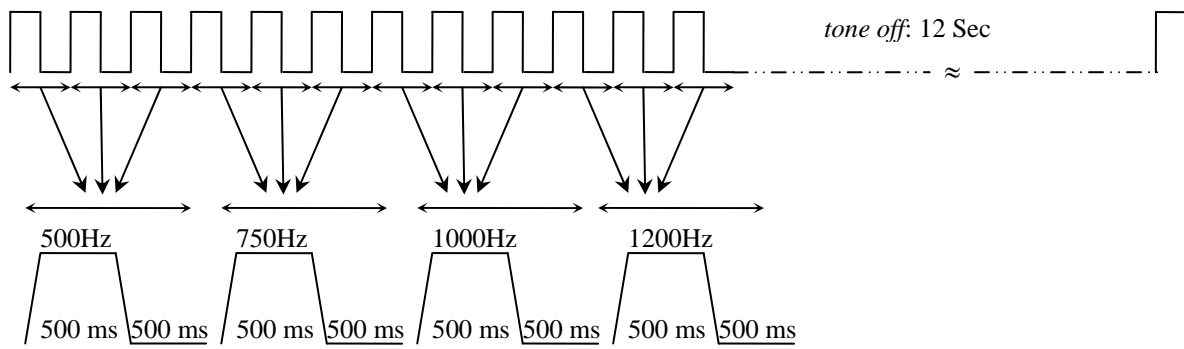


Fig. 14: Illustration of one epoch (block) of the stimulus profile for an auditory excitation. Each epoch contains 12 seconds of tones on and 12 second of tones off period. During the tones on period, 3 tone bursts were presented with a 15 ms rise/fall time at a rate of one per second for each of 4 tone frequencies 500Hz, 750 Hz, 1000 Hz, and 1200 Hz. MEG data of both subjects containe 50 epochs.

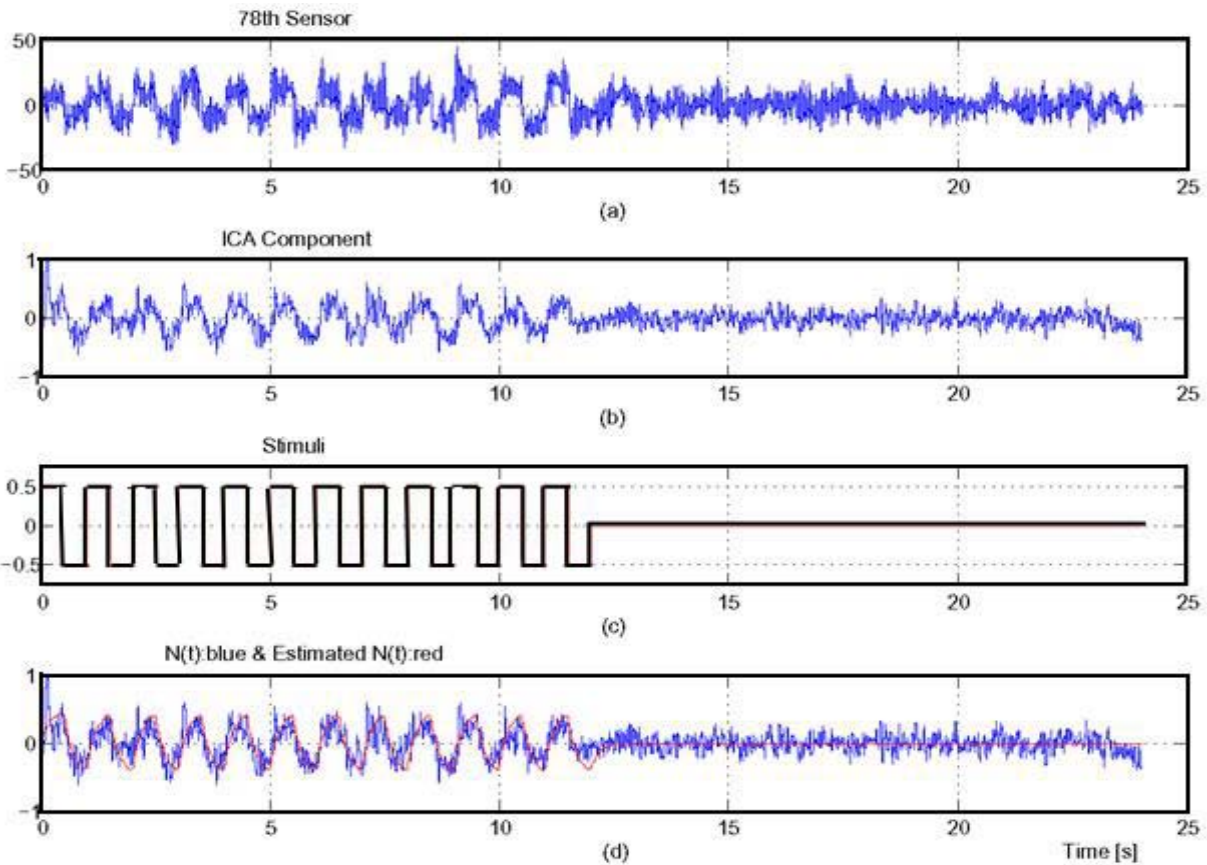


Fig. 15: Averaged MEG data and estimated model of the number of the active PSPs,  $N(t)$  for subject # 1. (a) Average MEG data over 50 blocks in the 78<sup>th</sup> sensor, which has strongest signal among all sensors. (b) The main ICA component averaged over 50 blocks. (c) Stimulus profile. (d)  $N(t)$  (blue plot) and its estimated model (red plot).

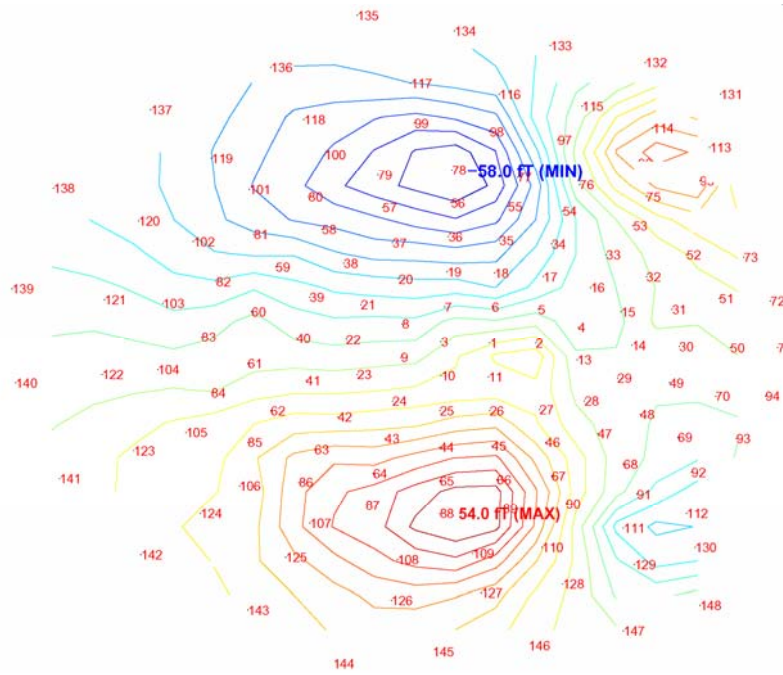


Fig. 16: Contour map of the amplitudes of the main ICA component (MEG data of subject # 1). The time course of the main ICA component is illustrated in Fig. 15-b.

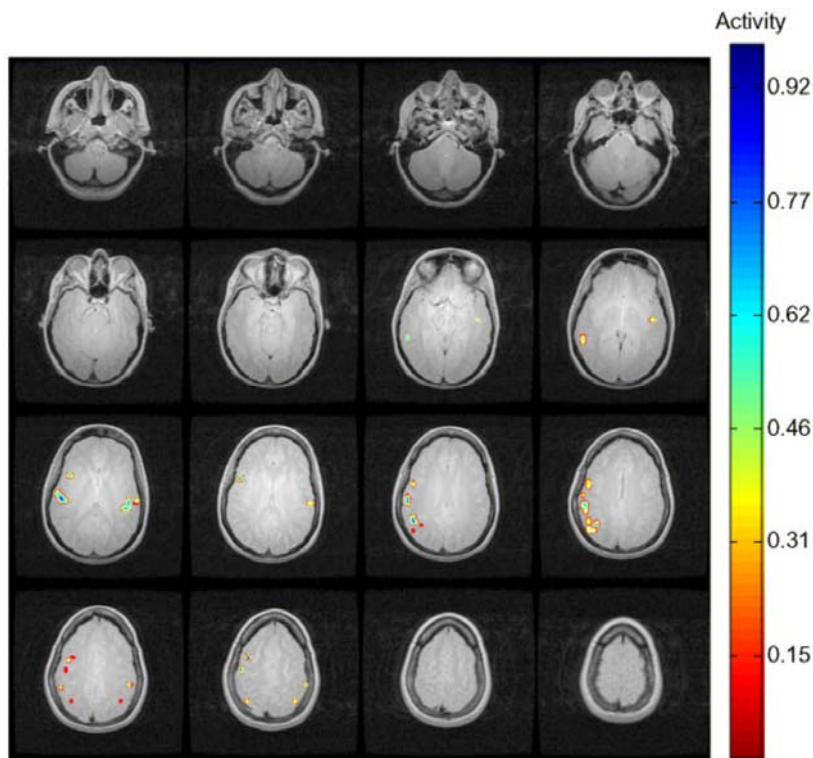


Fig. 17: Illustration of the detected activation from the fMRI data of subject # 2 co-registered to 3-D anatomical MRI data after removing single active voxels.

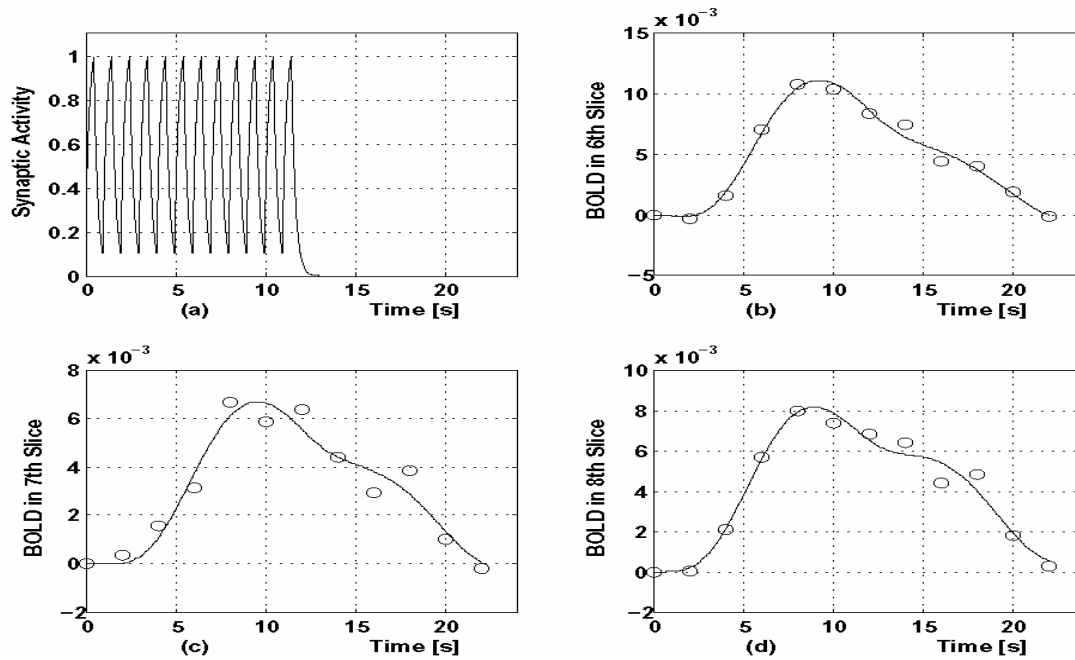


Fig.18: Number of active PSPs ( $N(t)$ ) and real and estimated BOLD responses (subject # 2). (a) Estimated  $N(t)$  as input of the EBM. (b) Real (-o- plot) and estimated BOLD signals of the 6<sup>th</sup> slice of fMRI volume where the average BOLD responses of all active voxels in the slice are used. (c) Same as (b) for the 7<sup>th</sup> slice. (d) Same as (b) for the 8<sup>th</sup> slice.

Table 1: stimulated values of the parameters of the proposed integrated model using real auditory data. The parameter  $T_p$ ,  $T_d$ , and  $K$  are related to the linear filter in Eq. (31). Parameters of the model which are related to the fMRI part of the model are according to Eqs. (2) and (18)-(20).

		Unit	Subject #1	Subject #2
MEC Parameters	$T_d$ (Afferent Delay)	ms	59	72
	$T_p$ (Time Constant of Linear Filter)	ms	44	31
	$K$	-	0.019	0.020
fMRI Parameters	$\sigma = [\sigma_x, \sigma_y, \sigma_z]$ (Spatial Crosstalk of fMRI)	mm	[ 7.5 , 7.5 , 5.5 ]	[ 10.0 , 10.0 , 7.0 ]
	$\varepsilon$ (Neural Efficiency)	-	0.13	0.15
	$\tau_s$ (Signal Decay)	s	20.05	25.36
	$\tau_f$ (Autoregulation)	s	3.45	3.75
	$\tau_0$ (Transit Time)	s	4.94	3.74
	$\alpha$ (Stiffness)	-	0.21	0.21
	$E_0$ (Oxygen Extraction)	-	0.67	0.57

data and the estimated  $N(t)$  is considered as the overall synaptic activity ( $\bar{u}(t)$  in Eq. (25)). Effect of the scalar coefficient between  $N(t)$  and  $\bar{u}(t)$  in (25) is considered in the neural efficiency ( $\epsilon$ ) in (18). The estimation process for the parameters of the EBM is started by choosing proper initial values. The “*fminsearch*” function, which uses the simplex search method, minimizes the sum square error between the real and estimated BOLD signals by iteratively changing the parameters of the EBM. “*Simulink*” is used to solve the nonlinear state-space equation (6) by the iterations of the “*fminsearch*” minimization. The estimated parameters of the EBM for both subjects are given in Table 1. Fig. 18 illustrates the real and estimated BOLD signals related to subject # 2.V. Summary and Conclusion

The purpose of this paper is to present an integrated MEG and fMRI model (Fig. 1). The MEG and fMRI BOLD signals are related to neural activities. The number of PSPs and APs show the overall neural activities. Based on the existing experimental studies and physiological facts, both MEG and fMRI signals are mainly related to PSPs and have almost no correlation with APs. The proposed stochastic model is based on the parameters of PSPs that are considered as random variables. In our model, the overall effect of PSPs is related to ECD in MEG and average neural activities as the input of the extended Balloon model in fMRI. Neural activities in a voxel can change CBF and produce BOLD signal in the neighboring voxels. We model this spatial blurring property of BOLD signal as “Crosstalk from Neural Activities of Adjacent Voxels.” The effects of model’s parameters are explored and illustrated using multiple simulation studies. These simulations show that the parameters of the model can explain conditions for which there is a detectable fMRI signal in a voxel but this voxel is silent for MEG and vice versa. Possible differences in the spatial responses of MEG and fMRI are also shown using our model (Figs. 11, 12 and 13). The crosstalk in fMRI and non-uniqueness property of the inverse problem in MEG are attributing sources for some of the differences in the spatial responses of the two modalities. We use real auditory MEG and fMRI datasets from 2 normal subjects to estimate the parameters of the model. Goodness of fit of the real data with our model suggests that the proposed model can be used in real conditions.

## References

[1] Almeida R, Stetter M (2002): Modeling the link between functional imaging and neuronal activity: synaptic metabolic demand and spike rates. *Neuroimage* 17:1065-1079.  
 [2] Ardekani B A and Kanno (1998): Statistical methods for detecting activated regions in functional MRI of the brain. *Magn. Reson. Imag.* 16(10):1217-1225.  
 [3] Attwell D, Iadecola C (2002): The neural basis of functional brain imaging signals. *Trends Neurosci* 25:621-625.  
 [4] Baillet S, Mosher JC, Leahy RM (2001): Electromagnetic Brain Mapping. *IEEE Signal Processing Magazine* 18:14-30.  
 [5] Babajani-Feremi Abbas (2006): Integrated model and Analysis of MEG and fMRI for Detection of Active Area in the

Brain. Doctorial dissertation, Electrical and Computer Engineering Faculty, University of Tehran, Iran.  
 [6] Babajani A and Soltanian-Zadeh H, (2006): Integrated MEG/EEG and fMRI model based on neural masses. *IEEE Trans. Biomed. Eng.* 53(9):1794-1801.  
 [7] Buxton RB, Wong EC, Frank LR (1998): Dynamics of blood flow and oxygenation changes during brain activation: the balloon mode. *Magn Reson Med* 39:855-864.  
 [8] Caesar K, Gold L, Lauritzen M (2003): Context sensitivity of activity dependent increases in cerebral blood flow. *Proc Natl Acad Sci USA* 100:4239-4244.  
 [9] Dale AM, Liu AK, Fisch BR (2000): Dynamic Statistical Parametric Mapping: Combining fMRI and MEG for High-Resolution Imaging of Cortical Activity. *Neuron* 26:55-67.  
 [10] David O, Harrison L, Friston K J, (2004): Modelling event-related responses in the brain. *Neuroimage* 25(3):756-770.  
 David O, Kiebel S J, Harrison L M, Mattout J, Kilner J M, [11]Friston K J., (2006): Dynamic causal modeling of evoked responses in EEG and MEG. *Neuroimage* 30(4):1255-1272.  
 [12] De Schutter E (1998): Dendritic voltage and calcium-gated channels amplify the variability of postsynaptic responses in a Purkinje cell model. *J Neurophysiol* 80:504-519.  
 [13] Friston KJ, Mechelli A, Turner R, Price CJ (2000): Nonlinear responses in fMRI: the Balloon model, Volterra kernels, and other hemodynamics. *Neuroimage* 12:466-477.  
 [14] Gulyas AI, Megias M, Emri Z, Freund TF (1999): Total number and distribution of inhibitory and excitatory synapses on hippocampal CA1 pyramidal cells. *J Neurosci* 19:10082-10097.  
 [15] Hämäläinen M, Hari R, Ilmoniemi RJ, Knuutila J, Lounasmaa OV (1993): Magnetoencephalography - theory, instrumentation and applications to noninvasive studies of the working human brain. *Rev of Modern Phys* 65:413-497.  
 [16] Heeger DJ, Huk AC, Geisler WS, Albrecht DG (2000): Spikes versus BOLD: what does neuroimaging tell us about neuronal activity?. *Nat Neurosci* 3:631-633.  
 [17] Heeger DJ, Ress D (2002): What does fMRI tell us about neuronal activity?. *Nat Rev Neurosci* 3:142-151.  
 [18] Horwitz B, Poeppel D (2002): How can EEG/MEG and fMRI/PET Data Be Combined? *Human Brain Mapping* 17:1-3.  
 [19] Iadecola C, Li J, Xu S, Yang G (1996): Neural mechanisms of blood flow regulation during synaptic activity in cerebellar cortex. *J Neurophysiol* 75:940-950.  
 [20] Iadecola C, Yang G, Ebner TJ, Chen G (1997): Local and propagated vascular responses evoked by focal synaptic activity in cerebellar cortex. *J Neurophysiol* 78:651-659.  
 [21] Jansen B H and Rit V G, (1995): Electroencephalogram and visual evoked potential generation in a mathematical model of coupled cortical columns. *Biol. Cybern.* 73:357-366.  
 [22] Jones M, Hewson-Stoate N, Martindale J, Redgrave P, Mayhew J (2004): Nonlinear coupling of neural activity and CBF in rodent barrel cortex. *Neuroimage* 22:956-965.  
 [23] Larkum ME, Launey T, Dityatev A, Luscher HR (1998): Integration of excitatory postsynaptic potentials in dendrites of motoneurons of rat spinal cord slice cultures. *J Neurophysiol* 80:924-935.  
 [24] Lauritzen M, Gold L (2003): Brain function and neurophysiological correlates of signals used in functional neuroimaging. *Jour Neurosci* 23:3972-3980.  
 [25] Liu AK, Belliveau JW, Dale AM (1998): Spatiotemporal imaging of human brain activity using functional MRI constrained magnetoencephalography data: Monte-Carlo simulations. *Proc Natl Acad Sci USA* 95:8945-8950.  
 [26] Liu AK, Dale AM, Belliveau JW (2002): Monte Carlo simulation studies of EEG and MEG localization accuracy.



Hum Brain Mapp 16:47-62.

[27] Logothetis NK (2002): The neural basis of the blood-oxygen-level-dependent functional magnetic resonance imaging signal. *Philos Trans R Soc Lond B Biol Sci* 357:1003-1037.

[28] Logothetis NK (2003): MR imaging in the non-human primate: studies of function and of dynamic connectivity. *Curr Opin Neurobiol* 13:630-642.

[29] Logothetis NK, Pauls J, Augath M, Trinath T, Oeltermann A (2001): Neurophysiological investigation of the basis of the fMRI signal. *Nature* 412:150-157.

[30] Martinez-Montes E, Valdes-Sosa PA, Miwakeichi F, Goldman RI, Cohen MS (2004): Concurrent EEG/fMRI analysis by multiway partial least squares. *NeuroImage* 22:1023-1034.

[31] Megias M, Emri Z, Freund TF, Gulyas AI (2001): Total number and distribution of inhibitory and excitatory synapses on hippocampal CA1 pyramidal cells. *Neuroscience* 102:527-540.

Miller KL, Luh WM, Liu TT, Martinez A, Obata T, Wong EC, Frank LR, Buxton RB (2001): Nonlinear temporal dynamics of the cerebral blood flow response. *Hum Brain Mapp* 13:1-12.

[33] Moran J E, Bowyer S M, Topley N, (2005): Multi-Resolution FOCUSS: A source imaging technique applied to MEG data. *Brain Topography* 18, 1-17.

[34] Nielsen AN, Lauritzen M (2001): Coupling and uncoupling of activity-dependent increases of neuronal activity and blood flow in rat somatosensory cortex. *J Physiol* 533:773-785.

[35] Nunez PL, Silberstein RB (2000): On the relationship of synaptic activity to macroscopic measurements: does co-registration of EEG with fMRI make sense?. *Brain Topography* 13:79-96.

[36] Rees G, Friston KJ, Koch C (2000): A direct quantitative relationship between the functional properties of human and macaque V5. *Nat Neurosci* 3:716-723.

[37] Riera J, Bosch J, Yamashita O, Kawashima R, Sadato N, Okada T, Ozaki T (2004): fMRI activation maps based on the NN-ARx model. *NeuroImage* 23:680-697.

[38] Riera J, Aubert E, Iwata K, Kawashima R, Wan X, Ozaki T (2005): Fusing EEG and fMRI based on a bottom-up model: Inferring activation and effective connectivity in neural masses. *Philosophical Transactions: Biological Sciences* 360(1457):1025-1041.

[39] Segev I (1998): Sound grounds for computing dendrites. *Nature* 393: 207-208.

[40] Sotero R C, Trujillo-Barreto N J, (2007): Biophysical model for integrating neuronal activity, EEG, fMRI and metabolism. *Neuroimage*. 39(1):290-309.

[41] Tsubokawa T, Katayama Y, T Kondo, Ueno Y, Hayashi N, Moriyasu N (1980): Changes in local cerebral blood flow and neuronal activity during sensory stimulation in normal and sympathectomized cats. *Brain Res* 190:51-64.

[42] Wang JZ, Williamson SJ, Kaufman L (1992): Magnetic Source Images Determined by a lead-Field Analysis: The Unique Minimum-Norm Least-Square Estimation. *IEEE Trans Biomed Eng* 39:665-675.